UNCLASSIFIED

SECURITY CLASSIFICATION OF THIS PAGE *(When Data Entered)*

REPORT DOCUMENTATION PAGE		READ INSTRUCTIONS BEFORE COMPLETING FORM
1. REPORT NUMBER RPI Math. Rep. No. 142	2. GOVT ACCESSION NO.	3. RECIPIENT'S CATALOG NUMBER
4. TITLE *(and Subtitle)* Influence of horizontally-random bottom structure on acoustic intensity in a shallow ocean		5. TYPE OF REPORT & PERIOD COVERED 6. PERFORMING ORG. REPORT NUMBER
7. AUTHOR(s) M. J. Jacobson, W. L. Siegmann, and C. E. Ashley		8. CONTRACT OR GRANT NUMBER(s) N00014-76-C-0288
9. PERFORMING ORGANIZATION NAME AND ADDRESS Rensselaer Polytechnic Institute Troy, New York 12181		10. PROGRAM ELEMENT, PROJECT, TASK AREA & WORK UNIT NUMBERS NR 386-606
11. CONTROLLING OFFICE NAME AND ADDRESS Office of Naval Research, Code 425 Department of the Navy Arlington, Virginia 22217		12. REPORT DATE 15 April 1984 13. NUMBER OF PAGES 43
14. MONITORING AGENCY NAME & ADDRESS*(if different from Controlling Office)*		15. SECURITY CLASS. *(of this report)* 15a. DECLASSIFICATION/DOWNGRADING SCHEDULE

16. DISTRIBUTION STATEMENT *(of this Report)*

This document has been approved for public release and sale; its distribution is unlimited.

17. DISTRIBUTION STATEMENT *(of the abstract entered in Block 20, if different from Report)*

18. SUPPLEMENTARY NOTES

19. KEY WORDS *(Continue on reverse side if necessary and identify by block number)*

Underwater Acoustics
Shallow-Water Acoustics
Random Ocean Bottoms
Intensity Variations

20. ABSTRACT *(Continue on reverse side if necessary and identify by block number)*

Effects of a model for random bottom structure on acoustic intensity in isospeed shallow water are studied. The randomness is due to stochastic variations in the bottom density and sound speed in the horizontal direction beneath a plane water-bottom interface. Ray geometry, spreading loss, and bottom loss and phase shift are examined in order to derive formulas for mean

- continued -

DD FORM 1 JAN 73 1473 EDITION OF 1 NOV 65 IS OBSOLETE
S/N 0102-LF-014-6601

UNCLASSIFIED

SECURITY CLASSIFICATION OF THIS PAGE *(When Data Entered)*

intensity and the variance of intensity. The expressions obtained are sufficiently general to permit their use with different bottom-acoustic models of sound reflection. In this paper, for illustrative and comparative purposes two such models, one developed by MacKenzie and the other by Rayleigh, are considered. The distinctive acoustic consequences of bottoms of different density mean, variance, and horizontal correlation are discussed, as are comparisons of results for the two bottom-reflection models. Intensity moments are obtained also for differing source-receiver range and water depth.

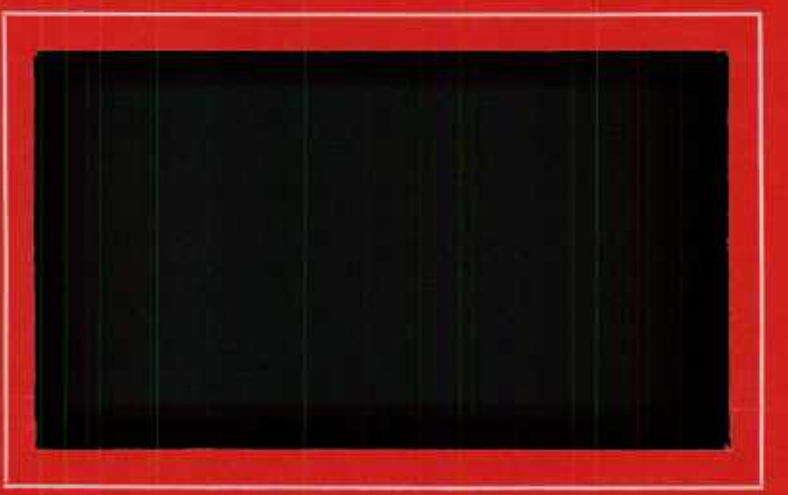

Rensselaer Polytechnic Institute

Troy, New York 12181

Influence of horizontally-random bottom structure on acoustic intensity in a shallow ocean

by

M. J. Jacobson, W. L. Siegmann
and C. E. Ashley

Department of Mathematical Sciences

Rensselaer Polytechnic Institute,

Troy, New York 12181

RPI Math. Rep. No. 142

April 15, 1984

This work was sponsored by

Code 425, Office of Naval Research

Contract No. N00014-76-C-0288

NR 386-606

ABSTRACT

Effects of a model for random bottom structure on acoustic intensity in isospeed shallow water are studied. The randomness is due to stochastic variations in the bottom density and sound speed in the horizontal direction beneath a plane water-bottom interface. Ray geometry, spreading loss, and bottom loss and phase shift are examined in order to derive formulas for mean intensity and the variance of intensity. The expressions obtained are sufficiently general to permit their use with different bottom-acoustic models of sound reflection. In this paper, for illustrative and comparative purposes two such models, one developed by MacKenzie and the other by Rayleigh, are considered. The distinctive acoustic consequences of bottoms of different density mean, variance, and horizontal correlation are discussed, as are comparisons of results for the two bottom-reflection models. Intensity moments are obtained also for differing source-receiver range and water depth.

INTRODUCTION

The acoustical effects of random interface topography between the water and bottom has been and is the object of much research. In contrast, the influence of random variations in bottom structure has received relatively less attention. One recent perspective on the influence of these two general types of bottom effects on acoustic propagation is found in Ref. 1. Both types of bottom variations are particularly important in shallow water.[2] Indeed, ocean regions may be regarded, for acoustic propagation studies, as shallow whenever sound transmission is significantly influenced by the bottom (see for instance Ref. 3). However, there is such an overabundance of bottom input parameters for intensity calculations and predictions that one model, or even several, seem inadequate to account for them all. For example, Rogers[4] lists twenty-four separate inputs to a propagation loss model for shallow-water acoustics. Furthermore, some of these parameters are so poorly known that it would not be feasible to model their acoustical effects. Therefore, it has been suggested (for example, see Ref. 4) that a statistical approach could possibly give reasonably accurate predictions for propagation loss. In this paper, we use such an approach to study how horizontal random variations in bottom density and sound speed affect sound transmission.

The specific problem we address assumes an ocean of shallow depth, so that the water can be assumed to have constant sound speed and density. A horizontal water-bottom interface is also assumed, and the bottom is taken to have small random variations in sound speed and density in the horizontal direction. Associated with these random quantities are correlations which depend upon the horizontal distance separating two locations. The ray theory of propagation is used in the water, and more than one reflection theory at the water-bottom interface is studied. Since shallow-water propagation is

dominated by repeated bottom interactions, we are necessarily considering ocean areas such as the continental terrace region where depths are less than about 200 m.[5] Our primary objective is to determine statistics of intensity at a fixed receiver, in terms of statistics of the bottom structure.

In Sec. I we derive expressions for per-ray travel time, geometrical spreading loss, bottom loss, and bottom phase shift. Rather general expressions for the mean intensity and its variance are developed in Sec. II, while Sec. III contains a specialization of the results when MacKenzie and Rayleigh bottom-loss models are used. The method by which bottom acoustic attenuation is incorporated, and the assumed type of horizontal bottom correlation function, are also discussed. Section IV presents and discusses numerical results obtained from the expressions we derived for the case of MacKenzie theory. In Sec. V, we compare those results obtained previously using MacKenzie theory with those employing Rayleigh theory. Finally, Sec. VI is a summary of the paper.

I. FORMULATION

We consider an isospeed ocean channel of constant depth, H, as suggested in Fig. 1(a). A point sound source S is located at a depth h_S and a point receiver R at depth h_R. The horizontal separation between S and R is denoted by R.

As stated in the introduction, ray theory is used here, and specular reflection at both surface and bottom is assumed. Rays are distinguished from each other by describing each by the ordered pair (n,j). Thus, a ray is denoted by r_{nj}, where $n \geq 0$ indicates the total number of bottom reflections between S and R. The symbol j specifies the type of ray, of which for $n \geq 1$ there are four, as illustrated in Fig. 1(b). For a ray that leaves S in a downward (or upward) direction and arrives at R from below, j is taken to be

one (or two). Similarly, j = 3 and j = 4 correspond to the other ray-direction pairs at S and R, as shown in the figure. For the special case n = 0, when $h_S < h_R$, j takes on the values 3 and 4 but not 1 and 2; when $h_S > h_R$, j can be 2 and 4 but not 1 and 3 [see Fig. 1(b)]. Each bottom reflection of the ray r_{nj} can be labeled by the unique triple (i,j,n), where i numbers each bounce sequentially from one to n. These three indices will be essential in describing two bottom parameters in our model. In particular, we let $\rho_{ij}^{(n)}$ and $c_{ij}^{(n)}$ denote the bottom density and sound speed at bottom bounce i of ray r_{nj}. The water density ρ_1 and the sound speed c_1 are taken constant. Returning to Fig. 1(a), the angle that ray r_{nj} makes with the horizontal as it leaves the source is denoted by θ_{nj}. Of course, this is also the magnitude of the inclination angle everywhere along r_{nj}. We define the inclination angle $-\frac{\pi}{2} < \theta_{nj} < \frac{\pi}{2}$ to be measured from the horizontal, and to be positive counterclockwise, as indicated in the figure.

The sound source S is taken to emit a unity-amplitude omnidirectional cw signal sin ωt, where ω is circular frequency and t is time. Then, ray r_{nj} arrives at the receiver after a time of travel T_{nj} in the form $A_{nj} \sin(\omega t - \theta_{nj})$. The relative per-ray amplitude A_{nj} differs from unity largely because of spreading loss and bottom loss, with other losses being neglected here. The per-ray travel time and phase shifts at surface and bottom reflections cause the phase ϕ_{nj} at the receiver to differ from that at the source. We may write

$$A_{nj} = \Lambda_{nj}^{-1/2} B_{nj} \tag{1}$$

and

$$\phi_{nj} = \omega T_{nj} - \left[n + \frac{1}{2}(\lambda+\nu)\pi\right] - \sum_{i=1}^{n} s_{ij}^{(n)} . \tag{2}$$

In Eq. (1), A_{nj} is spreading loss, given by

$$A_{nj} = P_{nj}^2 \ , \tag{3}$$

where P_{nj} is the length of r_{nj}. The quantity B_{nj} represents the decrease in amplitude due to all the bottom reflections of ray r_{nj}, and may be written

$$B_{nj} = \prod_{i=1}^{n} B_{ij}^{(n)} \ , \tag{4}$$

where $B_{ij}^{(n)}$ is the coefficient of reflection of r_{nj} at its ith bottom bounce. In Eq. (2),

$$T_{nj} = P_{nj}/c_1 \tag{5}$$

is travel time, while $S_{ij}^{(n)}$ represents the phase shift at the ith bottom reflection of r_{nj}. The symbol λ and ν are parameters defined by

$$\lambda = (2.5-j)/|2.5-j| \tag{6}$$

and

$$\nu = (-1)^j \ , \tag{7}$$

which account for surface reflections in the family of rays with n bottom bounces. From geometric considerations, a formula for path length of r_{nj} can be shown to be

$$P_{nj} = \left[R^2 + \left(2nH + \lambda h_R + \nu h_s\right)^2\right]^{1/2} \ . \tag{8}$$

Thus, A_{nj} is given through Eqs. (1), (3), (4), and (8), and ϕ_{nj} by Eqs. (2) and (5)-(8). Note that, if the source and receiver are located on the surface (i.e., $h_R = h_s = 0$), then Eq. (8) reduces to

$$P_{n1} = \left[R^2 + [2nH]^2\right]^{1/2} \ , \tag{9}$$

so that, in this particular case, the parameters λ and ν are not required.

Since the amplitudes of successive ray arrivals converge to zero with reasonable rapidity, because of increasing bottom and spreading losses, we need consider in total-field calculations only rays that experience some maximum number N or fewer bottom reflections. A typical condition to determine N, which we have used in our numerical examples, is to neglect rays which have amplitude less than one percent of the ray with largest amplitude. Consequently, the total acoustic field at R, of amplitude A and phase Φ, may be written in the form

$$A \sin(\omega t - \Phi) = \sum_{n=0}^{N} \sum_{j=1}^{4} A_{nj} \sin(\omega t - \phi_{nj}) \ . \tag{10}$$

It follows from Eq. (10) that A can be written in terms of the per-ray amplitudes and phases as

$$A^2 = \Big(\sum_{n=0}^{N} \sum_{j=1}^{4} A_{nj} \sin \phi_{nj} \Big)^2 + \Big(\sum_{n=0}^{N} \sum_{j=1}^{4} A_{nj} \cos \phi_{nj} \Big)^2 \ . \tag{11}$$

We shall employ Eq. (11) in Sec. II.

We turn now to expressions for $B_{ij}^{(n)}$ and $S_{ij}^{(n)}$, where bottom properties at the location of each ray reflection are taken to vary in a small random fashion about fixed "average" values. In our model we consider variations both in the density $\rho_{ij}^{(n)}$ of the bottom at the ith bounce of r_{nj} and in the sound speed $c_{ij}^{(n)}$ of the bottom at that point. Thus, we write

$$\rho_{ij}^{(n)} / \rho_1 = (\rho_2 / \rho_1)(1 + \varepsilon_{ij}^{(n)}) \ , \tag{12}$$

where ρ_2 is the constant horizontally-averaged density of the bottom, and $\varepsilon_{ij}^{(n)}$ is a small random quantity $(|\varepsilon_{ij}^{(n)}| << 1)$. In a similar manner, we let

$$c_1 / c_{ij}^{(n)} = (c_1 / c_2)(1 + \delta_{ij}^{(n)}) \ , \tag{13}$$

where c_2 is the constant mean sound speed in the bottom and $|\delta_{ij}^{(n)}| << 1$. In the next section, we will discuss the first and second moments of the random quantities $\varepsilon_{ij}^{(n)}$ and $\delta_{ij}^{(n)}$, including their correlation at pairs of points along the water-bottom interface.

We now expand the bottom loss $\mathcal{B}_{ij}^{(n)}$ in a Maclaurin series with respect to $\varepsilon_{ij}^{(n)}$ and $\delta_{ij}^{(n)}$, keeping only second and lower degree terms. It follows that

$$\mathcal{B}_{ij}^{(n)} = A_{nj} + B_{nj}\,\varepsilon_{ij}^{(n)} + C_{nj}\,\delta_{ij}^{(n)} + D_{nj}\left(\varepsilon_{ij}^{(n)}\right)^2 + E_{nj}\left(\varepsilon_{ij}^{(n)}\,\delta_{ij}^{(n)}\right) + F_{nj}\left(\delta_{ij}^{(n)}\right)^2 , \tag{14}$$

where the coefficients A_{nj} through F_{nj} depend on the reflection theory and mean bottom values that are selected. In Sec. IV we show explicit results for the reflection theories of MacKenzie and Rayleigh. Of course, other theories for which these equations are valid could also be utilized if desired. The per-ray bottom phase shift $S_{ij}^{(n)}$ may be expanded similarly to give:

$$S_{ij}^{(n)} = G_{nj} + H_{nj}\,\varepsilon_{ij}^{(n)} + I_{nj}\,\delta_{ij}^{(n)} + J_{nj}\left(\varepsilon_{ij}^{(n)}\right)^2 + K_{nj}\left(\varepsilon_{ij}^{(n)}\,\delta_{ij}^{(n)}\right) + L_{nj}\left(\delta_{ij}^{(n)}\right)^2 . \tag{15}$$

Again, the coefficients G_{nj} through L_{nj} in Eq. (15) are prescribed by the chosen reflection theory and unperturbed bottom density and sound speed.

II. INTENSITY MOMENTS

We turn now to a consideration of the mean and variance of the relative intensity I at R. In view of our definition of A, $I = A^2$ where A^2 is given in Eq. (11). Since the per-ray quantities A_{nj} and ϕ_{nj} in Eq. (11) depend on the random variables $\varepsilon_{ij}^{(n)}$ and $\delta_{ij}^{(n)}$ in Eqs. (12) and (13), I is necessarily a random variable. Our first objective is to express I in terms of these random variables.

We begin by expressing ϕ_{nj} from Eq. (2) in terms of quanitities $\bar{\Phi}_{nj}$ and γ_{nj}, where $\bar{\Phi}_{nj}$ does not depend upon the small stochastic perturbations $\varepsilon_{ij}^{(n)}$ and $\delta_{ij}^{(n)}$, while γ_{nj} does:

$$\phi_{nj} = \bar{\Phi}_{nj} + \gamma_{nj} \tag{16}$$

To second-degree terms, Eqs. (2), (5), (8), and (15) give

$$\bar{\Phi}_{nj} = \omega P_{nj}/c_1 - \left[n + \frac{1}{2}(\lambda+\nu)\right]\pi - n\, G_{nj} \tag{17a}$$

and

$$\gamma_{nj} = \sum_{i=1}^{n} \left[H_{nj}\, \varepsilon_{ij}^{(n)} + I_{nj}\, \delta_{ij}^{(n)} + J_{nj}\left(\varepsilon_{ij}^{(n)}\right)^2 + K_{nj}\left(\varepsilon_{ij}^{(n)}\, \delta_{ij}^{(n)}\right) + L_{nj}\left(\delta_{ij}^{(n)}\right)^2\right] . \tag{17b}$$

Next, we write A_{nj} as

$$A_{nj} = \bar{A}_{nj}\, \Gamma_{nj} \tag{18}$$

where similarly $\bar{A}_{nj}$ is independent of $\varepsilon_{ij}^{(n)}$ and $\delta_{ij}^{(n)}$ and Γ_{nj} is one when the small perturbations are zero. From Eqs. (1), (3), (4), and (14), we find

$$\bar{A}_{nj} = A_{nj}^{n}/P_{nj} \tag{19a}$$

and

$$\Gamma_{nj} = \prod_{i=1}^{n} \left[1 + \left(B_{nj}/A_{nj}\right)\varepsilon_{ij}^{(n)} + \left(C_{nj}/A_{nj}\right)\delta_{ij}^{(n)} + \left(D_{nj}/A_{nj}\right)\left(\varepsilon_{ij}^{(n)}\right)^2 + \left(E_{nj}/A_{nj}\right)\left(\varepsilon_{ij}^{(n)}\, \delta_{ij}^{(n)}\right) + \left(F_{nj}/A_{nj}\right)\left(\delta_{ij}^{(n)}\right)^2\right] . \tag{19b}$$

Substituting Eqs. (16) and (18) into Eq. (11), carrying out the squares, and combining terms, we obtain:

$$I = \sum_{n=0}^{N} \sum_{m=0}^{N} \sum_{j=1}^{4} \sum_{k=1}^{4} \bar{A}_{nj} \bar{A}_{mk} \Gamma_{nj} \Gamma_{mk} \cos\left(\bar{\Phi}_{nj} - \bar{\Phi}_{mk} + \gamma_{nj} - \gamma_{mk}\right) . \tag{20}$$

With an expression of the cosine that retains all terms to second order in the density and sound-speed perturbations, it follows from Eq. (20) that

$$I = \sum_{n=0}^{N} \sum_{m=0}^{N} \sum_{j=1}^{4} \sum_{k=1}^{4} \bar{A}_{nj} \bar{A}_{mk} \left\{\left[1 - \frac{1}{2}\left(\gamma_{nj} - \gamma_{mk}\right)^2\right]\Gamma_{nj} \Gamma_{mk} \right.$$

$$\left. \times \cos\left(\bar{\Phi}_{nj} - \bar{\Phi}_{mk}\right) + \left(\gamma_{nj} - \gamma_{mk}\right)\Gamma_{nj} \Gamma_{mk} \sin\left(\bar{\Phi}_{nj} - \bar{\Phi}_{mk}\right)\right\} . \tag{21}$$

Thus, the intensity is known from Eqs. (8), (17), (19), and (21), correct to second-order terms in $\varepsilon_{ij}^{(n)}$ and $\delta_{ij}^{(n)}$.

We are now in a position to determine the mean and variance of the intensity,

$$\mu(I) = E(I) \tag{22}$$

and

$$\sigma^2(I) = E(I^2) - E^2(I) , \tag{23}$$

where E denotes stochastic expectation. In doing so, we will take

$$E\left(\varepsilon_{ij}^{(n)}\right) = E\left(\delta_{ij}^{(n)}\right) = 0 , \tag{24}$$

$$\sigma^2\left(\varepsilon_{ij}^{(n)}\right) \equiv \sigma_{\varepsilon}^2 , \tag{25a}$$

and

$$\sigma^2\left(\delta_{ij}^{(n)}\right) \equiv \sigma_{\delta}^2 . \tag{25b}$$

Equations (25) mean that all $\varepsilon_{ij}^{(n)}$ and all $\delta_{ij}^{(n)}$ are assumed to have the same variance. Other second-order moments will be written as

$$E\left(\varepsilon_{ij}^{(n)}\ \varepsilon_{\ell k}^{(m)}\right) = \sigma_\varepsilon^2\ C\left(\varepsilon_{ij}^{(n)},\ \varepsilon_{\ell k}^{(m)}\right) , \tag{26a}$$

$$E\left(\delta_{ij}^{(n)}\ \delta_{\ell k}^{(m)}\right) = \sigma_\delta^2\ C\left(\delta_{ij}^{(n)},\ \delta_{\ell k}^{(m)}\right) , \tag{26b}$$

and

$$E\left(\varepsilon_{ij}^{(n)}\ \delta_{\ell k}^{(m)}\right) = \sigma_\varepsilon\ \sigma_\delta\ C\left(\varepsilon_{ij}^{(n)},\ \delta_{\ell k}^{(m)}\right) . \tag{26c}$$

In Eqs. (26) σ_ε and σ_δ are the standard deviations of $\varepsilon_{ij}^{(n)}$ and $\delta_{ij}^{(n)}$, introduced in Eqs. (25), and $C(a,b)$ represents the correlation coefficient of the random quantities a and b.

In calculating moments involving the $\delta_{ij}^{(n)}$, we employ for convenience an approximate relationship between bottom sound-speed and density perturbations. For small enough perturbations, it may be anticipated that $\varepsilon_{ij}^{(n)}$ and $\delta_{ij}^{(n)}$ are approximately proportional, which is confirmed by examination of data. In particular, from the extensive data in Table I of Ref. 6 and linear regression, or using appropriate equations from that reference, we found that to a good approximation,

$$\varepsilon_{ij}^{(n)} \doteq -\ 2\delta_{ij}^{(n)} . \tag{27}$$

This result can be used to write Eqs. (26b) and (26c) as

$$\sigma_\delta^2\ C\left(\delta_{ij}^{(n)},\ \delta_{\ell k}^{(m)}\right) = \frac{1}{4}\ \sigma_\varepsilon^2\ C\left(\varepsilon_{ij}^{(n)},\ \varepsilon_{\ell k}^{(m)}\right) \tag{28a}$$

and

$$\sigma_\varepsilon \sigma_\delta\ C\left(\varepsilon_{ij}^{(n)},\ \delta_{\ell k}^{(m)}\right) = -\ \frac{1}{2}\ \sigma_\varepsilon^2\ C\left(\varepsilon_{ij}^{(n)},\ \varepsilon_{\ell k}^{(m)}\right) , \tag{28b}$$

so that only the single correlation function $C\left(\varepsilon_{ij}^{(n)}, \varepsilon_{\ell k}^{(m)}\right)$ enters our calculations.

We can now perform the stochastic averaging and write expressions for $\mu(I)$ and $\sigma^2(I)$ from Eqs. (22) and (23), by use of Eqs. (17b), (19b), (21), (24)-(26), and (28). These formulas, while important to our analysis, are quite lengthy, and thus will not be presented here. Instead, we next further simplify the mean and variance of the intensity, which after the stochastic averaging still contain the functions $\cos(\bar{\Phi}_{nj}-\bar{\Phi}_{mk})$ and $\sin(\bar{\Phi}_{nj}-\bar{\Phi}_{mk})$. We do this by performing an average over those phase contributions which are independent of our stochastic bottom variations. This procedure is essentially equivalent to the process of obtaining incoherent total-field intensity. Specifically, we assume that the $\bar{\Phi}_{nj}$, and differences between them, are random and uniformly distributed over a 2π-radian interval. Performing such phase averages and denoting them by angular brackets, we obtain

$$\langle \mu(I) \rangle = \sum_{n=0}^{N} \sum_{j=1}^{4} \bar{A}_{nj}^2 \tag{29}$$

and

$$\begin{aligned} \langle \sigma^2(I) \rangle = & \sum_{n=0}^{N} \sum_{m=0}^{N} \sum_{j=1}^{4} \sum_{k=1}^{4} 2\sigma_\varepsilon^2 \bar{A}_{nj}^2 \bar{A}_{mk}^2 \times \\ & \left\{ \left[A_{nj}^{-2} \left(B_{nj} - \frac{1}{2} C_{nj} \right)^2 + \left(H_{nj} - \frac{1}{2} I_{nj} \right)^2 \right] \sum_{i=1}^{n} \sum_{\ell=1}^{n} C\left(\varepsilon_{ij}^{(n)}, \varepsilon_{\ell j}^{(n)}\right) \right. \\ & + \left[3A_{nj}^{-1} A_{mk}^{-1} \left(B_{nj} - \frac{1}{2} C_{nj} \right) \left(B_{mk} - \frac{1}{2} C_{mk} \right) - \left(H_{nj} - \frac{1}{2} I_{nj} \right) \times \right. \\ & \left. \left. \left(H_{mk} - \frac{1}{2} I_{mk} \right) \right] \sum_{i=1}^{n} \sum_{\ell=1}^{m} C\left(\varepsilon_{ij}^{(n)}, \varepsilon_{\ell k}^{(m)}\right) \right\} . \end{aligned} \tag{30}$$

It should be recalled that in Eqs. (29) and (30), n or m equal to zero is a special case with only two possible j values (see discussion at start of Sec. I).

Equations (29) and (30) represent the principal results of this section and will be analyzed in subsequent sections. At this point we content ourselves with two important observations. First, the mean intensity $\langle \mu(I) \rangle$ depends on mean per-ray amplitudes only, and does not vary with any of the bottom coefficients $B_{nj},\ldots,F_{nj},H_{nj},\ldots,L_{nj}$ from Eqs. (14) and (15). Second, the variance $\langle \sigma^2(I) \rangle$ depends only on the coefficients B_{nj}, C_{nj}, H_{nj}, and I_{nj} of linear terms in $\varepsilon_{ij}^{(n)}$ and $\delta_{ij}^{(n)}$ in Eqs. (14) and (15). That is, even though the variance is a second-order quantity in the density and sound-speed perturbations, and even though six coefficients of second-order terms (i.e., D_{nj}, E_{nj}, F_{nj}, J_{nj}, K_{nj}, and L_{nj}) are retained in calculating Eqs. (29) and (30), our final results are independent of these coefficients. This is a significant simplification, since these six coefficients represent certain higher-order information about the acoustic response of the bottom, which is thus not required for our intensity results.

III. BOTTOM MODELING

Having derived formulas for the mean intensity $\langle \mu(I) \rangle$ and variance $\langle \sigma^2(I) \rangle$, stochastically averaged over random bottom variations and incoherently averaged over per-ray phase, we wish to use them with two models of bottom reflection.

We consider first MacKenzie's model,[7] in which bottom loss is

$$\mathcal{B}_{ij}^{(n)} = \left[\left(h_+ - \sigma \sin \theta_{nj}\right)^2 + h_-^2\right]^{1/2}\left[\left(h_+ + \sigma \sin \theta_{nj}\right)^2 + h_-^2\right]^{-1/2} , \qquad (31a)$$

and bottom phase shift is

$$S_{ij}^{(n)} = \tan^{-1}\left\{2\sigma h_- \sin \theta_{nj}\left[\sigma^2 \sin^2 \theta_{nj} - \left(h_+^2 + h_-^2\right)\right]^{-1}\right\} . \qquad (31b)$$

In Eqs. (31)

$$h_{\pm} = \left\{\pm g + \left[(\alpha/\beta)^2 + g^2\right]^{1/2}\right\}^{1/2} , \tag{32a}$$

$$g = \frac{1}{2}\left[1 - (v_2/c_1)^2 \cos^2\theta_{nj} - (\alpha/\beta)^2\right] , \tag{32b}$$

$$\cos\theta_{nj} = R/P_{nj} , \tag{32c}$$

and

$$\sigma = \rho_{ij}^{(n)} \, v_2/\rho_1 c_1 . \tag{32d}$$

The quantity v_2 is the phase speed of acoustic waves in the bottom and, to an excellent approximation,[7] $v_2 \doteq c_{ij}^{(n)}$. The term α/β is a factor that accounts for attenuation in the bottom, and in fact, α is often referred to as the attenuation coefficient. This quantity provides a dissipative mechanism for sound which enters the bottom and is typically a function of bottom density. However, since the values of α/β are usually extremely small[8] compared to other quantities in our formulas for $\langle\mu(I)\rangle$ and $\langle\sigma^2(I)\rangle$, we may reasonably express α/β in terms of the mean density ρ_2, rather than in terms of $\rho_{ij}^{(n)}$. That is, the perturbation factor $\varepsilon_{ij}^{(n)}$ in $\rho_{ij}^{(n)}$ is negligible in α/β. We now turn to a model for the dependence of this quantity on ρ_2.

Hamilton[9] gives an expression $k_p\omega/2\pi$ for α in terms of a quantity k_p, which characterizes natural saturated surface sediments, and the circular acoustic frequency ω. His findings are presented in the form of scatter diagrams and regression curves for k_p versus porosity. Since porosity can be expressed fairly accurately in terms of bottom density,[9] we can obtain expressions for k_p in terms of ρ_2. We found from Hamilton's results that:

$$k_p = 1.1096 - 0.3058\ \rho_2 , \tag{33a}$$

for coarse, medium, and fine sand;

$$k_p = 5.9990 - 2.845\ \rho_2 , \tag{33b}$$

for very fine sand and lower porosity mixed-size sand;

$$k_p = -4.4240 + 2.837\ \rho_2 \ , \tag{33c}$$

for mixed-size sand; and

$$k_p = 0.3622 - 0.5712\ \rho_2 + 0.2626\ \rho_2^2 \ , \tag{33d}$$

for silt-clay bottoms. The quantity β is given by[7] $\omega/c_{ij}^{(n)}$, and consistent with our earlier approximation, we may write

$$\alpha/\beta = k_p c_{ij}^{(n)}/2\pi \doteq k_p c_2/2\pi \ . \tag{34}$$

Note that α/β from Eqs. (33) and (34) is independent of frequency. Other investigators have proposed different models for attenuation,[10,11] and they could also be used if desired.

From our bottom model, we must obtain the coefficients A_{nj}, $B_{nj} - C_{nj}/2$, and $H_{nj} - I_{nj}/2$ for use in Eq. (30). It follows from Eqs. (31) and (32) and our assumption on α/β [see Eqs. (33) and (34)] that the variations $\varepsilon_{ij}^{(n)}$ and $\delta_{ij}^{(n)}$ in $\rho_{ij}^{(n)}$ and $c_{ij}^{(n)}$ only enter Eqs. (31) and (32) through the quantities $c_{ij}^{(n)}/c_1$ in Eq. (32b) and the σ in Eq. (32d). This latter parameter is sometimes referred to as the impedance ratio, i.e. the ratio of acoustic impedance of the bottom to that of the water. Thus, we write $c_1/c_{ij}^{(n)}$ and $\rho_{ij}^{(n)}/\rho_1$ as in Eqs. (12) and (13), and with Eq. (27), we can express $c_{ij}^{(n)}/c_1$ and σ in terms of $\delta_{ij}^{(n)}$ and the mean sound-speed and impedance ratios

$$\overline{c} = c_2/c_1 \tag{35a}$$

and

$$\overline{\sigma} = \rho_2 c_2/\rho_1 c_1 \ . \tag{35b}$$

In addition we relate the bottom sound speed c_2 (in m/s) in our model to ρ_2 (in g/cm^3) by the relation[6]

$$c_2(\rho_2) = 2270.9 - 1194.4\ \rho_2 + 474.6\ \rho_2^2 \ . \tag{35c}$$

We then expand Eqs. (31a), (32a), and (32b) in a Maclaurin series in $\delta_{ij}^{(n)}$. With the notation of Eq. (14), we find

$$A_{nj} = M_{nj}^{-}/M_{nj}^{+} \ , \tag{36a}$$

and

$$C_{nj} - 2B_{nj} = \left[Q_{nj}^{+}/\left(M_{nj}^{-}M_{nj}^{+}\right) - Q_{nj}^{-}\ M_{nj}^{-}/\left(M_{nj}^{+}\right)^3\right]/2 \ , \tag{36b}$$

where

$$M_{nj}^{\pm} = \left[2T_{nj} \pm 2\bar{\sigma}\ R_{nj}^{+}\ \sin\theta_{nj} + \bar{\sigma}^2\ \sin^2\theta_{nj}\right]^{1/2} \ , \tag{36c}$$

$$Q_{nj}^{\pm} = \left(\bar{c}^2\ \cos^2\theta_{nj}\right)\left(S_{nj}/T_{nj}\right) - 6\bar{\sigma}^2\ \sin^2\theta_{nj}$$

$$+ \bar{\sigma}\ R_{nj}^{+}\ \sin\theta_{nj}\left[\left(\bar{c}^2\cos^2\theta_{nj}\right)/T_{nj} \pm 6\right] \ , \tag{36d}$$

$$R_{nj}^{\pm} = \left[T_{nj} \pm S_{nj}/2\right]^{1/2} \ , \tag{36e}$$

$$T_{nj} = \left[\left(\alpha/\beta\right)^2 + S_{nj}^2/4\right]^{1/2} \ , \tag{36f}$$

and

$$S_{nj} = 1 - \bar{c}^2\cos^2\theta_{nj} - \left(\alpha/\beta\right)^2 \ . \tag{36g}$$

These coefficients, though lengthy, present no difficulty for numerical evaluations. In a similar way, we find from Eqs. (31b), (32a), and (32b) that

$$I_{nj} - 2H_{nj} = \left[\left(-X_{nj}U_{nj} + V_{nj}W_{nj}\right)/\left(U_{nj}^2 + W_{nj}^2\right)\right] \ , \tag{37a}$$

$$U_{nj} = \bar{\sigma}^2\sin^2\theta_{nj} - 2T_{nj} \ , \tag{37b}$$

$$V_{nj} = \bar{c}^2\cos^2\theta_{nj}\left(S_{nj}/T_{nj}\right) + 6\bar{\sigma}^2\sin^2\theta_{nj} \ , \tag{37c}$$

$$W_{nj} = 2\bar{\sigma}\ R_{nj}^{-}\sin\theta_{nj} \ , \tag{37d}$$

and

$$X_{nj} = \bar{\sigma}\ R_{nj}^{-}\sin\theta_{nj}\left[\left(\bar{c}^2\cos^2\theta_{nj}\right)/T_{nj} + 6\right] \ . \tag{37e}$$

A second and simpler bottom-reflection model is that obtained from the classical theory of Rayleigh.[12] Indeed, Rayleigh bottom loss and phase shift can be found from the corresponding MacKenzie results, Eqs. (31) and (32), by setting $\alpha/\beta = 0$. In this case, the bottom loss can be written as

$$\mathcal{B}_{ij}^{(n)} = \{(\rho_{ij}^{(n)}/\rho_1) - [(c_1/c_{ij}^{(n)})^2 - \cos^2\theta_{nj}]^{1/2}[1 - \cos^2\theta_{nj}]^{-1/2}\}$$

$$\times \{(\rho_{ij}^{(n)}/\rho_1) + [(c_1/c_{ij}^{(n)})^2 - \cos^2\theta_{nj}]^{1/2}[1 - \cos^2\theta_{nj}]^{-1/2}\}^{-1} ,$$

$$\theta_c < \theta < \pi/2 , \tag{38a}$$

and

$$\mathcal{B}_{ij}^{(n)} = 1 , \qquad 0 < \theta < \theta_c . \tag{38b}$$

For the bottom phase shift, we may write

$$S_{ij}^{(n)} = 2\tan^{-1}\{[\rho_1\cos^2\theta_{nj}$$

$$- (c_1/c_{ij}^{(n)})^2]^{1/2}[\rho_2(1-\cos^2\theta_{nj})^{1/2}]^{-1/2}\}, \quad 0 < \theta < \theta_c , \tag{39a}$$

and

$$S_{ij}^{(n)} = 0 , \qquad \theta_c < \theta < \pi/2 . \tag{39b}$$

In Eqs. (38) and (39), the critical angle is defined by[12]

$$\cos\theta_c = c_1/c_{ij}^{(n)} , \tag{40}$$

and θ_{nj} is given by Eq. (32c).

Once again, by writing $c_1/c_{ij}^{(n)}$ and $\rho_{ij}^{(n)}/\rho_1$ as in Eqs. (12) and (13) and using Eq. (27), we can expand Eqs. (38)-(40) in a Maclaurin series in $\delta_{ij}^{(n)}$ as done for the MacKenzie model. This procedure determines the quantities $(B_{nj}-C_{nj}/2)/A_{nj}$ and $H_{nj}-I_{nj}/2$ which appear in Eq. (30). We do not display these results because they can be obtained from the case $\alpha/\beta = 0$ of Eqs. (36) and (37).

For evaluation of the intensity variance $\langle\sigma^2(I)\rangle$ in Eq. (30), we also need the correlation coefficient in Eq. (28). For convenience we will use the Gaussian form[13]

$$C\left(\varepsilon_{ij}^{(n)},\varepsilon_{k\ell}^{(m)}\right) = \exp\left\{-\left[\left(x_{ij}^{(n)} - x_{k\ell}^{(m)}\right)/L\right]^2\right\} , \tag{41}$$

where $\left(x_{ij}^{(n)} - x_{k\ell}^{(m)}\right)$ is the horizontal distance between the ith bottom reflection of ray r_{nj} and the kth bottom bounce of ray $r_{m\ell}$. The parameter L is called the correlation length, which is the value of $\left|x_{ij}^{(n)} - x_{k\ell}^{(m)}\right|$ where C takes the value of 1/e. Of course, correlation functions other than that in Eq. (41) could be used, if desired or if suggested by bottom data.

IV. MACKENZIE-BOTTOM RESULTS

We now discuss some results obtained using our expressions, Eqs. (29) and (30), for mean intensity, $\langle\mu(I)\rangle$, and intensity variance, $\langle\sigma^2(I)\rangle$. Equations (33) and (34) were used to determine values for α/β, Eqs. (36) and (37) for coefficients in Eq. (30), and the correlation coefficient in Eq. (41) was employed. For convenience, our numerical results were determined with the source and receiver located on the surface. Of course, other configurations could have been used. In all our computations, we found that all rays were included up to a maximum number N of 6 or 7 bottom bounces, according to the criterion stated in Sec. I. Rays with more bottom interactions were shown to negligibly affect our results.

Graphs of the function

$$M_R = 10 \log_{10} \langle\mu(I)\rangle/\langle\sigma(I)\rangle \tag{42}$$

appear in Figs. 2 and 3 and will be discussed shortly. In addition, graphs of intensity ratios I_R, where this symbol is used to denote both

$$I_R = 10 \log_{10} \langle\mu(I)\rangle/\langle\mu_0(I)\rangle \tag{43a}$$

and

$$I_R = 10 \log_{10}\left(\langle\mu(I)\rangle \pm \langle\sigma(I)\rangle\right)/\langle\mu_0(I)\rangle \ , \qquad (43b)$$

are considered in Figs. 4-7. The moment ratio M_R is the ratio in dB of mean intensity to the standard deviation of intensity. It can be thought of as a signal-to-noise ratio, in the sense that a small (i.e., a large negative) value of M_R means that the fluctuation in intensity is large relative to the mean; a large value corresponds to the standard deviation being small compared to the mean. Equation (43a) is a normalized dB-measure of intensity, in which the term $\langle\mu_0(I)\rangle$ is taken to be the mean intensity for a bottom density with the particular value $\rho_2 = 1.80 g/cm^3$. This value corresponds to a typical silty-sand bottom. In Eq. (43b), $\langle\mu_0(I)\rangle$ has the same interpretation as in Eq. (43a); Eq. (43b) itself is a normalized dB-measure of intensity spread. That is, the two expressions in Eq. (43b) describe the amount of intensity variation within one standard deviation of the mean, where the mean is given by Eq. (43a). A small difference in the values of the two quantities in Eq. (43b) indicates that the fluctuations in intensity are small, while a large difference suggests a significant fluctuation.

Figure 2 is a plot of the moment ratio, Eq. (42), versus mean bottom density ρ_2. The values used for ρ_2 are typical of a bottom on the continental shelf. Density and sound-speed values in the water were taken to be $\rho_1 = 1.025\ g/cm^3$ and $c_1 = 1523$ m/s. In this figure, as in all our graphs except Fig. 7, we have chosen $\sigma_\varepsilon = 0.1$. This relation was made from an examination of Table I of Ref. 6. However, it should be pointed out that, due to the manner in which σ_ε^2 appears in Eq. (30), graphs of M_R would merely be shifted vertically if σ_ε were assigned a different value. Thus, the shapes and relative values of the curves would not be altered. In Fig. 2, we have taken L/H = 1, so that the bottom correlation length has been selected to be equal to the

water depth. Other numerical calculations, some of which are discussed in connection with a later figure, have explored the relatively small influence of different values for L/H.

Figure 2, then, illustrates the behavior of mean intensity as a function of mean bottom density, for four values of range-to-depth ratio R/H. We observe that M_R does not appear to exhibit a well-defined behavior as R/H changes. However, values of the moment ratio can be substantially different for different aspect ratios R/H. For example, when $\rho_2 = 1.6/cm^3$, the M_R value for R/H = 10 exceeds that for R/H = 5 by about 8 dB. All M_R versus ρ_2 curves exhibit a general upward trend, indicating that the mean intensity tends to increase as mean bottom density increases. As an illustration, M_R increases by nearly 20 dB as ρ_2 increases from 1.55 to 2.10 g/cm^3. As described earlier, this behavior suggests a much greater fluctuation in received intensity for a low-density bottom, such as one composed of silty clay. Rogers[4] obtained the same anomalous type of conclusion using an algebraic model for propagation loss. Specifically, his loss model is based on a combination of information from Weston,[14] Urick,[15] and McPherson and Daintith.[16] However, Ref. 4 utilizes a combination of ray and mode theories of propagation over a deterministic bottom, while we employ ray propagation over a horizontally random bottom. Returning to Fig. 2, one way to explain the increase in M_R with ρ_2 is to consider properties of MacKenzie reflection theory.[7] In particular, the change in bottom loss $\beta_{ij}^{(n)}$ and bottom phase shift $s_{ij}^{(n)}$ with increasing grazing angle is much greater for slow (low density) bottoms than for fast (high density) bottoms. This is particularly true for small ray angles, which are dominant in isospeed channels with large aspect ratios. Thus, these greater changes would account for larger values of $\langle\sigma(I)\rangle$ relative to values of $\langle\mu(I)\rangle$ when ρ_2 is small.

In Fig. 3 we have kept the aspect ratio constant (R/H = 20) and varied L/H, in graphs of moment ratio versus mean bottom density. It is readily observed that as ρ_2 increases, M_R exhibits an overall increasing trend. When the normalized correlation length is taken as L/H = 1, for example, M_R is observed to increase by about 14 dB as ρ_2 increases from 1.42 to 2.10 g/cm^3.

We also find little dependence of M_R on L/H, although the moment ratio tends to be larger for smaller L/H values when ρ_2 is large. However, M_R does not behave monotonically with L/H. As L becomes progressively larger, the correlation coefficient, Eq. (41), increases. Thus, for a small value of L, the correlation between random bottom properties at two points is small, and the fluctuations $\varepsilon_{ij}^{(n)}$ in the densities at these points tend to cancel. Consequently, $\langle\sigma(I)\rangle$ decreases, causing M_R to increase with L when L is small, as suggested by the L/H = 0 and 1 curves in Fig. 3. On the other hand, for larger L, there is more of a density relationship at two bottom points. The reduction in fluctuations will not occur to as great an extent as for small L, so that the value of $\langle\sigma(I)\rangle$ tends to be larger for larger L. This results in a decrease in M_R with increasing L, as observed in the L/H = 10 and ∞ curves of Fig. 3. Indeed, in our model, L/H = ∞ corresponds to a horizontally-uniform bottom of density which is unknown but is close to ρ_2. Finally, we note that calculations with R/H values other than 20 were found to have little gross effect on the behavior of M_R with ρ_2 for the selected L/H values.

Figures 4 through 7 are graphs of intensity ratios, as given in Eqs. (43). As we discussed just following that equation, these ratios illustrate the amount of spread in intensity predicted by our model for different values of ρ_2, R/H, and L/H. The quantity $\langle\mu_0(I)\rangle$ is the mean intensity for mean bottom density ρ_2 = 1.80g/cm^3, and is used as the reference value in the dB plots.

In Figs. 4 and 5, the normalized bottom correlation length is unity, but the aspect ratio R/H is 5 in the former figure and 20 in the latter. The dashed curves describe mean intensity, and the vertical separation between solid curves represents the amount of intensity fluctuation within one standard deviation about the mean. In both figures, the dashed intensity curves show a general upward trend as ρ_2 increases, indicating that mean intensity increases as the bottom becomes increasingly fast. Both figures show that intensity variation is much greater for lower density bottoms than for higher density ones. This is consistent with our previous discussion of Fig. 2. In Fig. 4, for example, the spread between the $\langle\mu(I)\rangle \pm \langle\sigma(I)\rangle$ curves is nearly 10 dB when $\rho_2 = 1.70$. The spread in values of intensity (solid curves) tends to be greater in Fig. 5 than in Fig. 4, so that intensity variation appears to increase with R/H.

Figure 6 displays the effect on intensity ratios of the normalized correlation length L/H. Increasing the length is seen to widen the dB interval in which intensity is within one standard deviation of its mean. Again, we attribute this to the cancelling of fluctuations in bottom density, as discussed in conjunction with Fig. 3. For example, when $\rho_2 = 1.90$, the spread is 3.5 dB as L/H approaches zero, but is about 6.0 dB as L/H becomes very large. Changing the value of L appears to have a slightly greater effect for transmission over higher density bottoms. In slow bottoms the effects of large changes in bottom loss $\delta_{ij}^{(n)}$ and phase shift $s_{ij}^{(n)}$ with grazing angle, discussed previously, causes the large interval between the $\langle\mu\rangle \pm \langle\sigma\rangle$ curves.

The effect on intensity variation of changing σ_ε, the standard deviation of bottom-density variations in Eq. (25a), is illustrated in Fig. 7. Here, L/H and R/H are held constant, and σ_ε is assigned four different values. Increasing σ_ε is observed to cause widening of the spread of the intensity distribution.

This is reasonable since $\langle\sigma\rangle$ increases with σ_ε, causing a greater variance of the signal intensity. As an example, the one-standard-deviation spread increases from 0 dB when $\sigma_\varepsilon = 0$ to about 13 dB when $\sigma_\varepsilon = 0.20$, for $\rho_2 = 1.80 g/cm^3$. The zero intensity value corresponding to $\sigma_\varepsilon = 0$ results, of course, from the fact that there is no intensity fluctuation when the bottom has constant density. Finally, we note that the effect of increased σ_ε is greatest when dealing with low density bottoms.

V. RAYLEIGH-BOTTOM RESULTS

Up to this point, we have used MacKenzie reflection theory in examining the effects of bottom-structure variations on received acoustic intensity. In Figs. 8 and 9, however, we compare intensity results using both MacKenzie and Rayleigh bottom models. The former employs our expansions Eqs. (36) and (37) of Eqs. (31) and (32), while the latter uses analogous expansions of Eqs. (38) and (39). In Fig. 8 we plot the moment ratio M_R, Eq. (42), versus ρ_2 for R/H = 5 (solid curves) and 20 (dashed curves), while fixing L/H at the value one. The heavy curves, which appeared previously in Fig. 2, are the results for the MacKenzie bottom model. The light curves correspond to the Rayleigh-theory bottom. In Fig. 9 we plot M_R versus ρ_2 for L/H = 0 (solid) and L/H $\to \infty$ (dashed), when R/H is fixed.

We observe that the light-dashed curves in Figs. 8 and 9, and the light-solid curve in Fig. 9, approach vertical asymptotes at several values of ρ_2. The light-solid curve in Fig. 8 has a single vertical asymptote. In contrast, moment-ratio curves for a MacKenzie bottom do not exhibit this behavior. A brief explanation of these asymptotes is appropriate here. It is known that for $c_2 > c_1$ and $\rho_2 > \rho_1$, the Rayleigh bottom reflection coefficient increases to a value of unity as the angle of incidence varies from normal to the critical angle θ_c. At angles more grazing than θ_c, the relative amplitude of the

reflected wave remains one, but there is a phase change between the reflected and incident waves, given by Eqs. (40).[12] It follows from Eqs. (32c) and (40) that

$$\left[\left(R/P_{nj}\right)^2 - \left(c_1/c_2\right)^2\right] = 0 \tag{44a}$$

when the critical angle θ_c is attained. Equation (44a) is equivalent to

$$c_2 = c_1\left[1 + \left(2nH/R\right)^2\right]^{1/2} , \tag{44b}$$

where we have used the path-length formula, Eq. (9). In our expansions of $\mathcal{B}_{ij}^{(n)}$ and $S_{ij}^{(n)}$, Eqs. (38) and (39), the left side of Eq. (44a) occurs in the denominators of the terms C_{nj} and I_{nj}. Thus, for given number n of bottom reflections and given range R, a value of c_2 (and hence of ρ_2, since they are related by Eq. (35c)) can occur for which C_{nj} and I_{nj} become infinite. This feature is also apparent in the graphs of $\mathcal{B}_{ij}^{(n)}$ and $S_{ij}^{(n)}$, where it is manifested as the infinite slopes at the critical angle.[12] Therefore, asymptotes of the M_2 versus ρ_2 curves in Figs. 8 and 9 result from our expansions in $\varepsilon_{ij}^{(n)}$ and $\delta_{ij}^{(n)}$, which are not valid at the critical angle. Because C_{nj} and I_{nj} become infinite, so does $\langle\sigma\rangle$, so that M_R expressed in dB approaches negative infinity. If the exact (and more complicated) dependence on $\varepsilon_{ij}^{(n)}$ and $\delta_{ij}^{(n)}$, rather than our linear approximations, were in some asymptotic manner retained in $\mathcal{B}_{ij}^{(n)}$ and $S_{ij}^{(n)}$, then the moment-ratio results would not be expected to possess discontinuities in values and slopes. Instead, it would be anticipated that M_R in dB would still exhibit sharp decreases at certain ρ_2 values, but these decreases would not become infinite. We remark also that as R/H increases, more asymptotes (corresponding to different n values) appear in the M_R versus ρ_2 curve, as implied by Eq. (44b).

Many of the same features pointed out in the discussion of Fig. 2 can be seen in Fig. 8. For instance, we observe that M_R exhibits a rather complicated

behavior as R/H changes, for either MacKenzie or Rayleigh theory. However, the values of the moment ratio can be quite different for different R/H values. For example, when $\rho_2 = 1.85$, the Rayleigh M_R value for R/H = 5 exceeds that for R/H = 20 by about 8 dB. The difference at the same ρ_2 value using the MacKenzie curves is about 5 dB. Apart from the previously-noted discontinuities in the Rayleigh curves, there are some general qualitative similarities in the curves for the two bottom theories. One illustration is the overall shapes of the two solid curves for R/H = 5. Also, we see that except for low-density bottoms, M_R tends to increase as ρ_2 increases. This same trend holds for the MacKenzie curves. For R/H = 5, the peak Rayleigh value in Fig. 8 is about 14 dB higher at $\rho_2 = 2.10$ than at $\rho_2 = 1.76$, indicating again the generally larger fluctuation in received intensity for low-density bottoms.

In Fig. 9, we have taken R/H = 20 and have graphed the limiting cases when L/H approaches zero and infinity. Of course, the MacKenzie curves are the same as two of those appearing in Fig. 3. There is a substantial difference between bottoms with ρ_2 less than about 1.55 and those above this value. For $\rho_2 >$ 1.55, MacKenzie results are always greater than those with Rayleigh, for both L/H values; below this value, the opposite is true. For example, if L/H = 0 and $\rho_2 = 1.45$, the moment ratio for a Rayleigh bottom is about 4 dB greater than that for the MacKenzie model. However, at $\rho_2 = 2.05$ and L/H = 0, the MacKenzie M_R is about 2 dB more than the corresponding Rayleigh value. In all four curves, a small correlation length L corresponds to less variance in intensity, as discussed in conjunction with Fig. 3. Some bottom-model consistency appears in Fig. 9, in the sense that dB-difference between the two solid curves (L/H=0) are approximately equal to dB-differences between the two dashed curves ($L/H=\infty$) at the peaks of the Rayleigh graphs. For example, at $\rho_2 = 1.87$, there is nearly a 2 dB difference between both the L/H = 0 and the $L/H = \infty$ curves.

The MacKenzie results in both Figs. 8 and 9 show vestiges of the discontinuities that appear in the approximate Rayleigh curves. These appear as local minima at values of ρ_2 where Rayleigh asymptotes occur. Indeed, if α/β were allowed to approach zero, the MacKenzie minima would progressively deepen. Thus, our intensity results reflect the proper relationship between the two bottom models. The MacKenzie model is commonly regarded as the more sophisticated of the two since it incorporates an additional physical effect (attenuation). Although certain relationships between the intensity results for these two bottom models have been described and illustrated, it is also true that the levels of corresponding curves show some definite differences. For example, the solid curves in Fig. 9 (corresponding to L/H = 0) demonstrate that, when comparing peak values of the Rayleigh curves with their MacKenzie equivalents, there may be up to 2 dB differences between the two. Thus, the physical features which are properly incorporated into the bottom model can be important in determining the values of the intensity moments.

VI. SUMMARY

In this paper we study the ramifications of horizontal random fluctuations in bottom structure on the intensity of a received acoustic signal. A shallow-water sound channel, having constant sound speed and density, is assumed and ray theory is used. The water-bottom interface is taken to be a plane horizontal surface, and the ocean bottom has random density and sound-speed fluctuations in the horizontal direction with a degree of relationship which varies with distance. For this stochastic bottom, we derive expressions for ray path length, spreading loss, travel time, and bottom loss and phase shift. Expressions for the latter two quantities are developed exploiting perturbation expansions, assuming small fluctuations in bottom density and sound speed.

Using these results, we find the mean acoustic intensity and variance of the intensity for a cw signal propagating in the shallow ocean channel. Stochastic averaging over bottom randomness and incoherent averaging over per-ray phases are performed to obtain the intensity moments. The results are sufficiently general that a variety of bottom-acoustic models can be employed with them. Also, the intensity moments are modeled to contain an arbitrary horizontal bottom correlation coefficient.

To illustrate our results, we chose bottom-reflection models of MacKenzie and Rayleigh. In order to use MacKenzie theory, a procedure was devised to specify values for the attenuation coefficient. Also, our numerical results assume a bottom coefficient of correlation of Gaussian form.

A number of conclusions are drawn from our calculations. For example, we find that the standard deviation of received intensity is less for sound transmission over fast (high density) bottoms than over slow (low density) bottoms. Also, when dealing with fast bottoms, i.e. mean densities over 1.76 g/cm^3, the ratio of mean intensity to standard deviation in dB (moment ratio) increases as source-receiver range R decreases. The same conclusion cannot be drawn for slow bottoms, where no distinctive pattern exists. In general, we find that the moment ratio increases as mean bottom density increases.

It is shown that, due to a cancelling of bottom density fluctuations, the standard deviation of intensity increases as the correlation length L increases. This effect is a consequence of the features of our model. We find also that varying L/H (H is water depth) does not have as great an effect on the moment ratio as does varying the channel aspect ratio R/H.

We examine two quantities, normalized dB-measures of intensity and intensity spread, in order to determine when received intensity is within one standard deviation of its mean value. We find that a greater spread of intensity

values can be expected over a low-density bottom than over a high-density bottom. Also, the spread in expected intensity values about the mean increases with R/H.

We observe that, for a given water depth H, shortening the correlation length L narrows the interval in which the intensity is within one standard deviation of its mean. It is also shown that increasing the standard deviation of bottom density fluctuations causes a widening of the spread of intensity values.

Statistics of intensity using the Rayleigh model are compared with those found using MacKenzie theory. The two bottom-reflectivity models give results that are sometimes similar. However, one of the sharpest differences is the presence of deep fades in moment ratio, for some mean bottom densities, when calculations are performed for the Rayleigh bottom. These occur when the inclination angle of an acoustic-ray arrival in the total field approaches the critical angle, in which case the variance of intensity becomes very large. Such a behavior, with comparable magnitude, is not observed when a MacKenzie bottom model is used.

[1] W. A. Kuperman and F. B. Jensen, Eds., Bottom-Interacting Ocean Acoustics (Plenum, New York, 1980).

[2] O. F. Hastrup and O. V. Oleson, "Sound Propagation in Shallow Water", SACLANTCEN Conference Proceedings No. 14, NATO SACLANT ASW Research Center, La Spezia (1974).

[3] F. Ingenito, R. H. Ferris, W. A. Kuperman, and S. N. Wolf, "Shallow-Water Acoustics Summary Report (First Phase)", Naval Research Lab., Washington, D. C., NRL Rep. 8179 (1978).

[4] P. H. Rogers, "Onboard Prediction of Propagation Loss in Shallow Water", Naval Research Lab., Washington, D.C., NRL Rep. 8500 (1981).

[5] A. P. Lisitzin, Sedimentation in the World Ocean (George Banta, Menasha, 1972) pp. 18-19.

[6] E. L. Hamilton, J. Geophysical Res. 75, 4423-4446 (1970).

[7] K. V. MacKenzie, J. Acoust. Soc. Am. 32, 221-231 (1960).

[8] E. L. Hamilton, J. Acoust. Soc. Am. 28, 1-15 (1956).

[9] E. L. Hamilton, Geophysics 37, 620-646 (1972).

[10] M. A. Biot, J. Acoust. Soc. Am. 28, 168-178 (1956).

[11] J. M. Hovem, J. Acoust. Soc. Am. 67 1559-1563 (1980).

[12] C. B. Officer, Introduction to the Theory of Sound Transmission (McGraw-Hill, New York, 1958) pp. 76-82.

[13] J. S. Bendat, Principles and Applications of Random Noise Theory (Wiley, New York, 1958) pp. 18-22.

[14] D. E. Weston, J. Acoust. Soc. Am. 42, 526-527 (1967).

[15] R. J. Urick, "A Prediction Model for Shallow Water Sound Transmission", Naval Ordnance Lab., Silver Spring, NOLTR 67-12 (1967).

[16] J. D. McPherson and M. J. Daintith, J. Acoust. Soc. Am. 41 850-860 (1967).

FIGURE LEGENDS

Fig. 1 (a) A horizontal isospeed channel and the geometry of a ray.

(b) Four possible ray configurations for n = 1 bottom reflections.

Fig. 2 Moment ratio M_R versus mean bottom density ρ_2 for four R/H ratios: L/H = 1, σ_ε = 0.1, c_1 = 1523 m/s, ρ_1 = 1.025 g/cm^3. Surfaced source and receiver.

Fig. 3 Moment ratio M_R versus mean bottom density ρ_2 for four L/H ratios: R/H = 20. Other parameters as in Fig. 2.

Fig. 4 Intensity ratio I_R versus mean bottom density ρ_2: L/H = 1, R/H = 5. Other parameters as in Fig. 2.

Fig. 5 Intensity ratio I_R versus mean bottom density ρ_2: L/H = 1, R/H = 20. Other parameters as in Fig. 2.

Fig. 6 Intensity ratio I_R versus ρ_2 for two L/H ratios: R/H = 20. Other parameters as in Fig. 2.

Fig. 7 Intensity ratio I_R versus ρ_2 for four σ_ε values: L/H = 1, R/H = 20. Other parameters as in Fig. 2.

Fig. 8 Moment ratio M_R versus mean bottom density ρ_2 using MacKenzie theory (heavy curves) and Rayleigh theory (light curves) for R/H = 5 (solid) and 20 (dashed): L/H = 1. Other parameters as in Fig. 2.

Fig. 9 Moment ratio M_R versus ρ_2 using MacKenzie theory (heavy curves) and Rayleigh theory (light curves) for L/H = 0 (solid) and ∞ (dashed): R/H = 20. Other parameters as in Fig. 2.

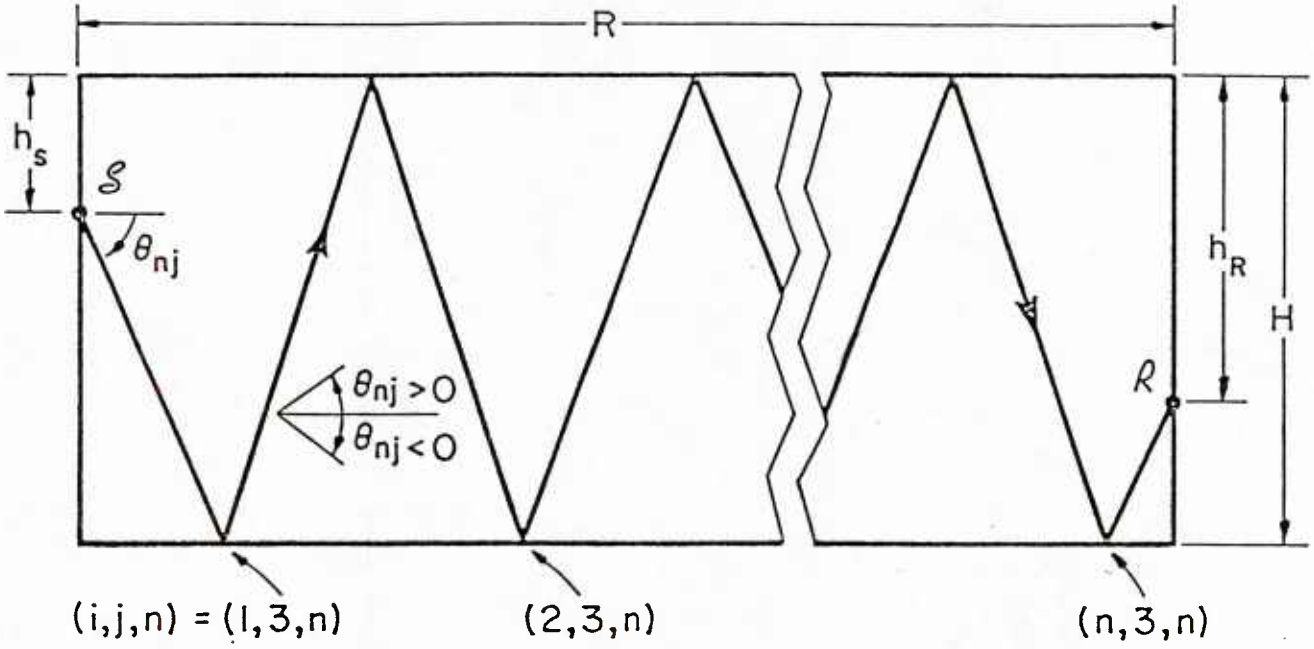
R
h_s
S
θ_{nj}
$\theta_{nj} > 0$
$\theta_{nj} < 0$
h_R
H
R
(i,j,n) = (1,3,n)
(2,3,n)
(n,3,n)

(a)

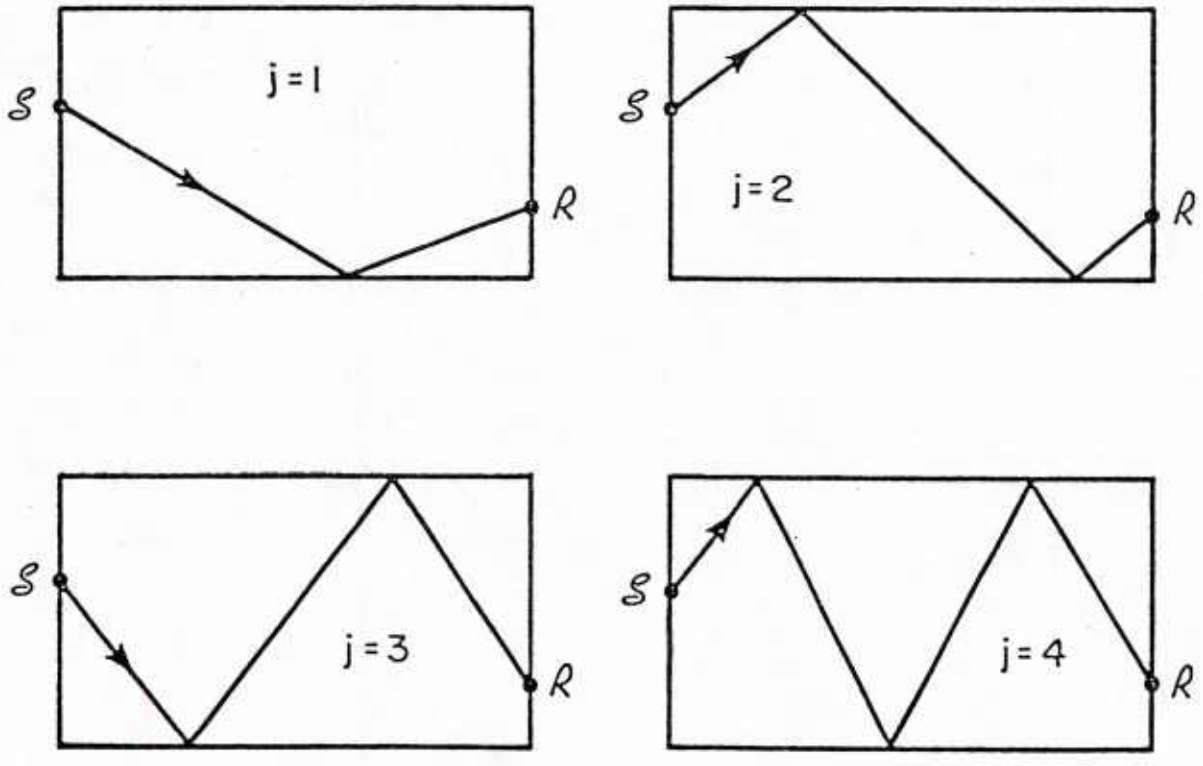
S
j=1
R
S
j=2
R
S
j=3
R
S
j=4
R

(b)

FIGURE 1

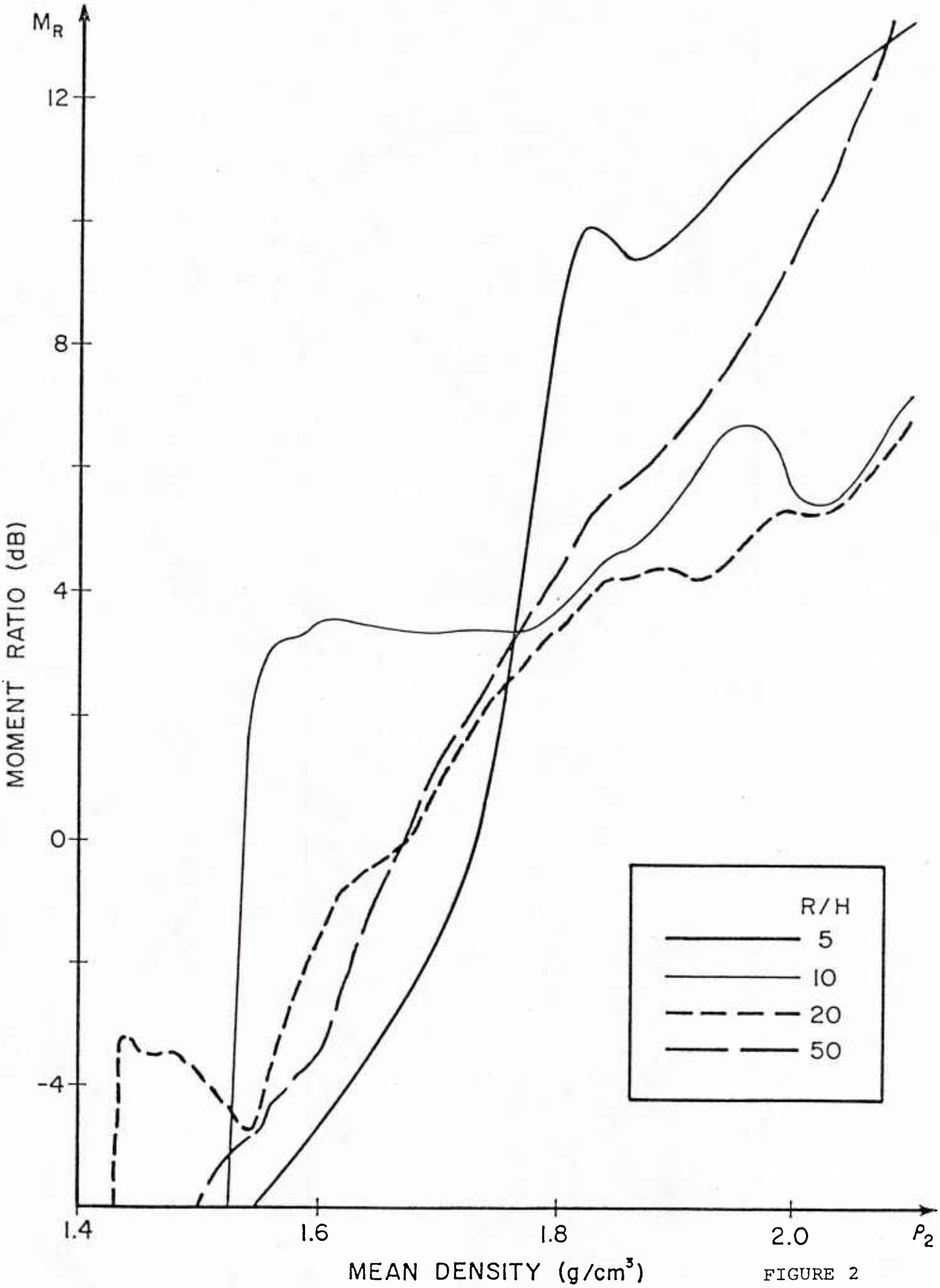
M_R
12
8
4
0
-4
MOMENT RATIO (dB)
1.4
1.6
1.8
2.0
ρ_2
MEAN DENSITY (g/cm³)
R/H
5
10
20
50

FIGURE 2

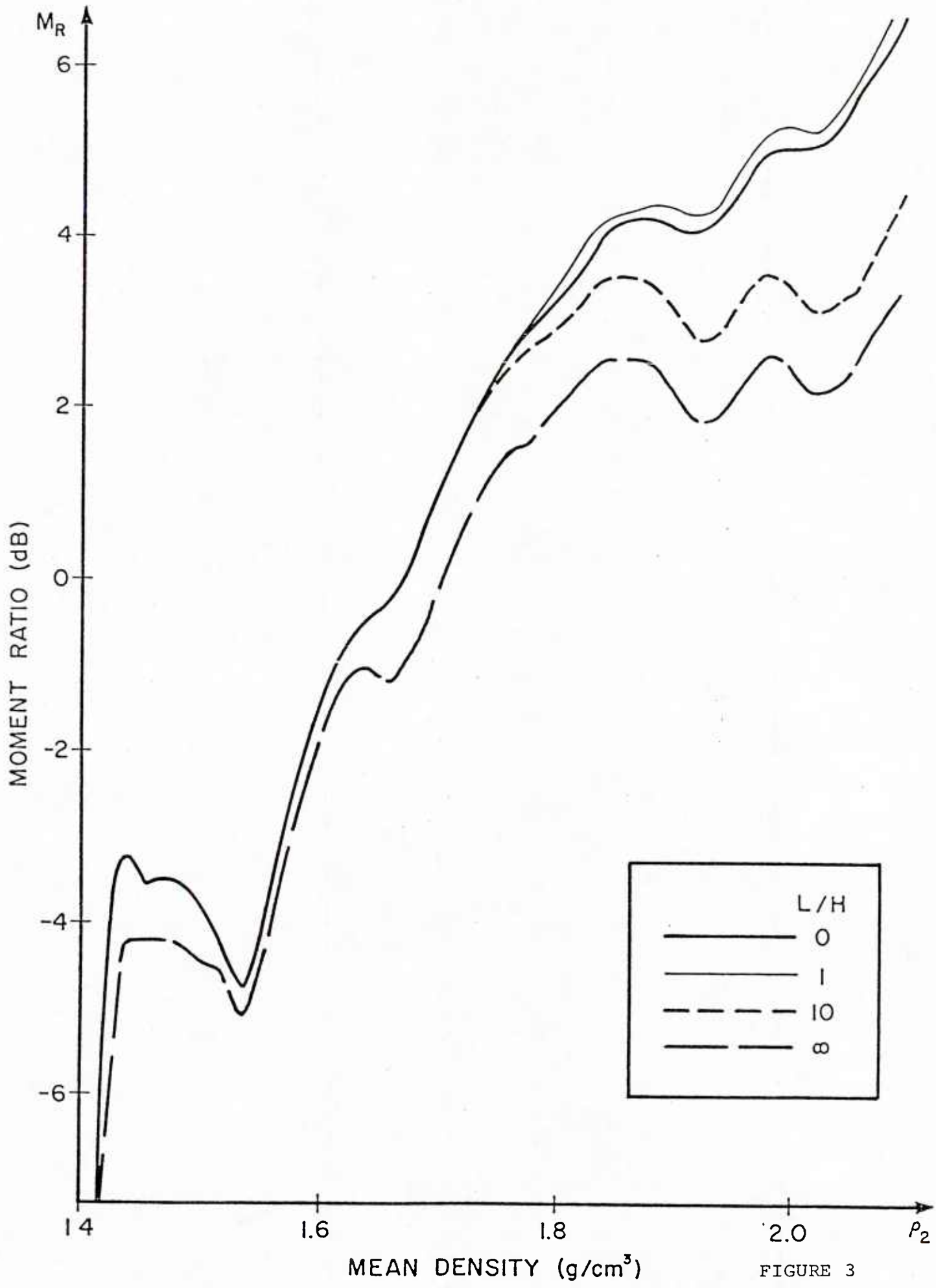
M_R
6
4
2
0
-2
-4
-6
MOMENT RATIO (dB)
1.4
1.6
1.8
2.0
ρ_2
MEAN DENSITY (g/cm^3)
L/H
0
1
10
∞

FIGURE 3

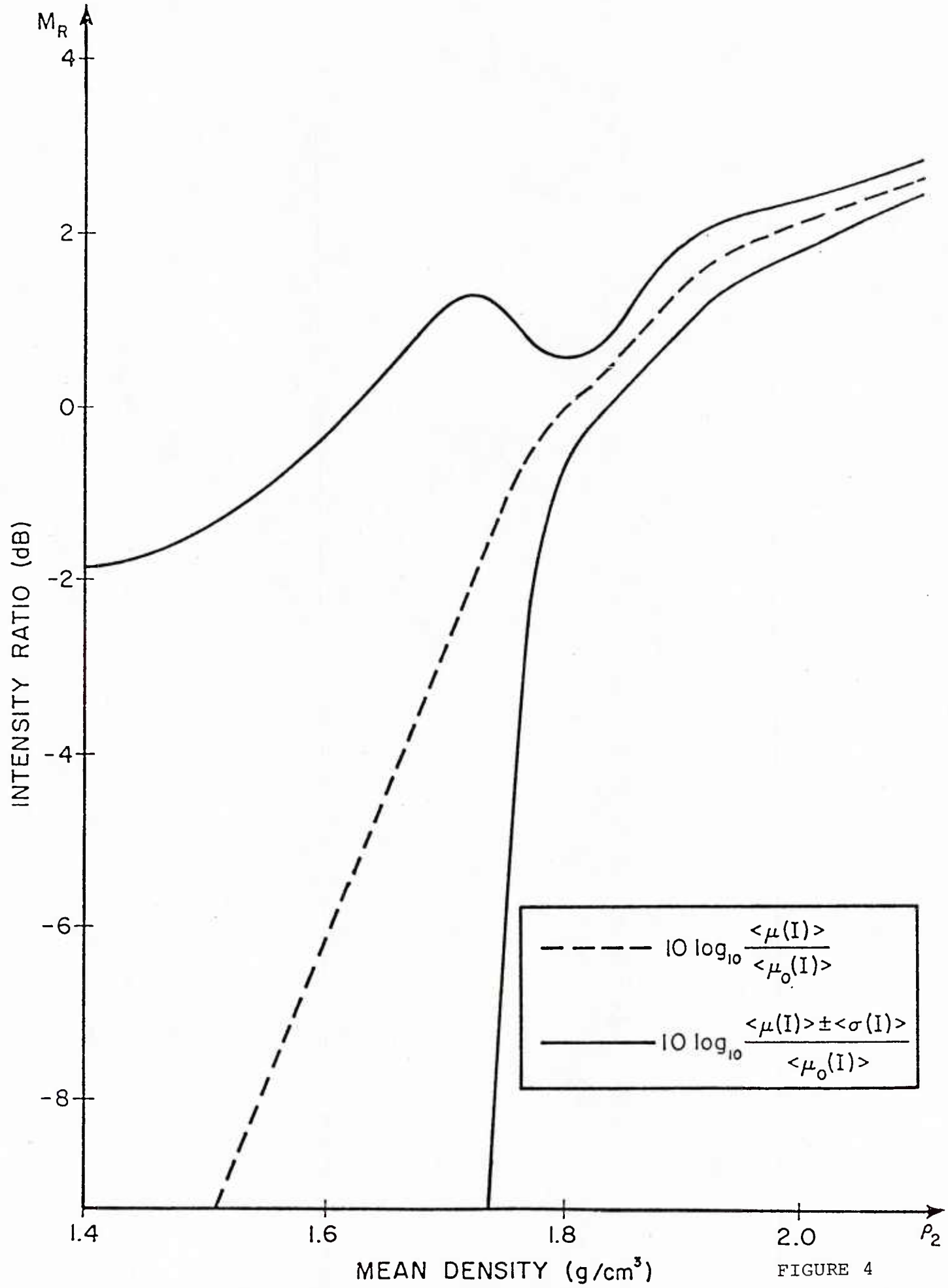
M_R
4
2
0
-2
-4
-6
-8
INTENSITY RATIO (dB)
1.4
1.6
1.8
2.0
ρ2
MEAN DENSITY (g/cm³)
10 log10 <μ(I)> / <μ0(I)>
10 log10 <μ(I)>±<σ(I)> / <μ0(I)>

FIGURE 4

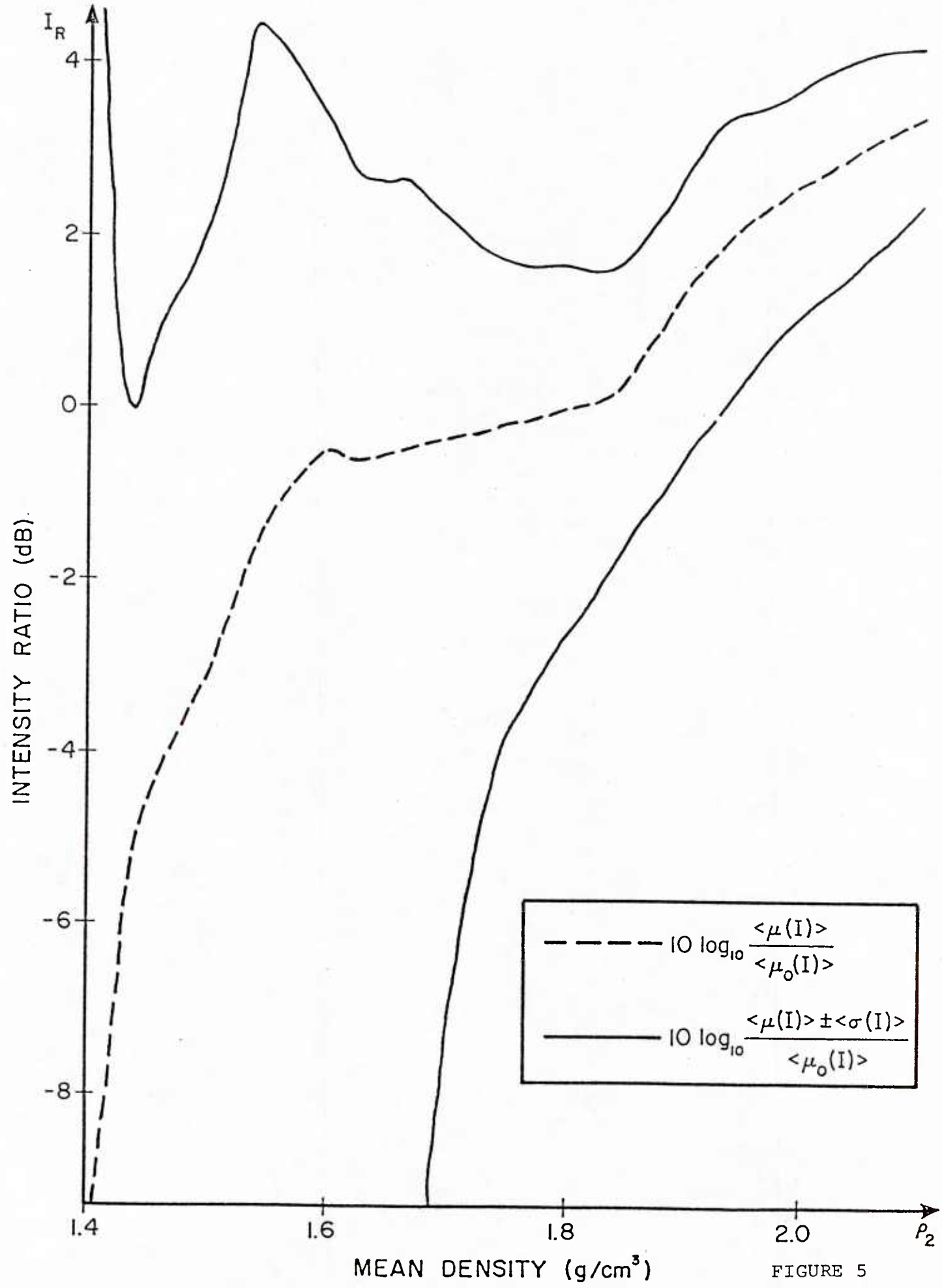
I_R
4
2
0
-2
-4
-6
-8
INTENSITY RATIO (dB)
1.4
1.6
1.8
2.0
ρ_2
MEAN DENSITY (g/cm³)
$10 \log_{10} \frac{\langle \mu(I) \rangle}{\langle \mu_0(I) \rangle}$
$10 \log_{10} \frac{\langle \mu(I) \rangle \pm \langle \sigma(I) \rangle}{\langle \mu_0(I) \rangle}$

FIGURE 5

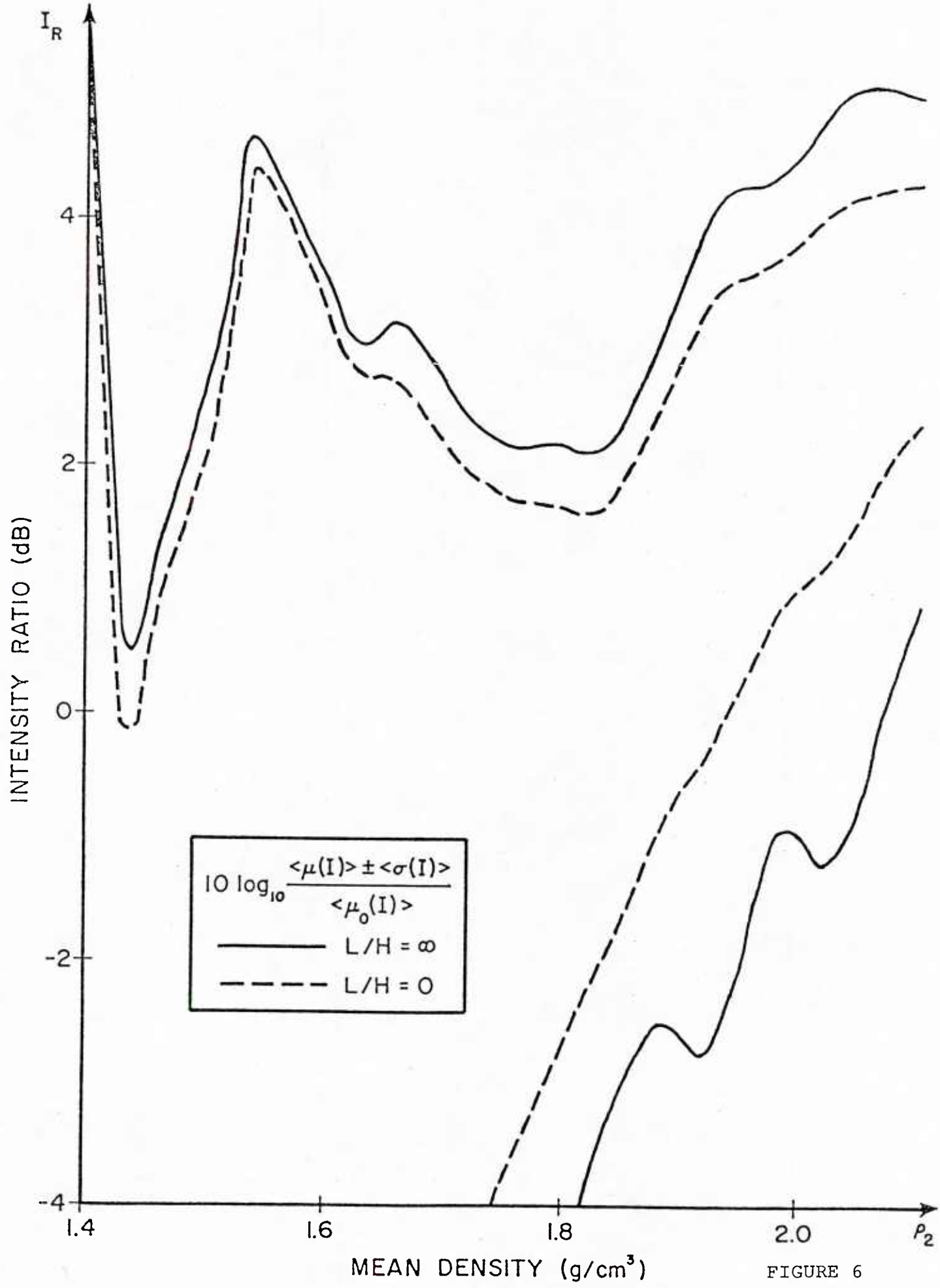
I_R
4
2
0
-2
-4
INTENSITY RATIO (dB)
$10 \log_{10} \frac{\langle \mu(I) \rangle \pm \langle \sigma(I) \rangle}{\langle \mu_0(I) \rangle}$
L/H = ∞
L/H = 0
1.4
1.6
1.8
2.0
ρ_2
MEAN DENSITY (g/cm³)

FIGURE 6

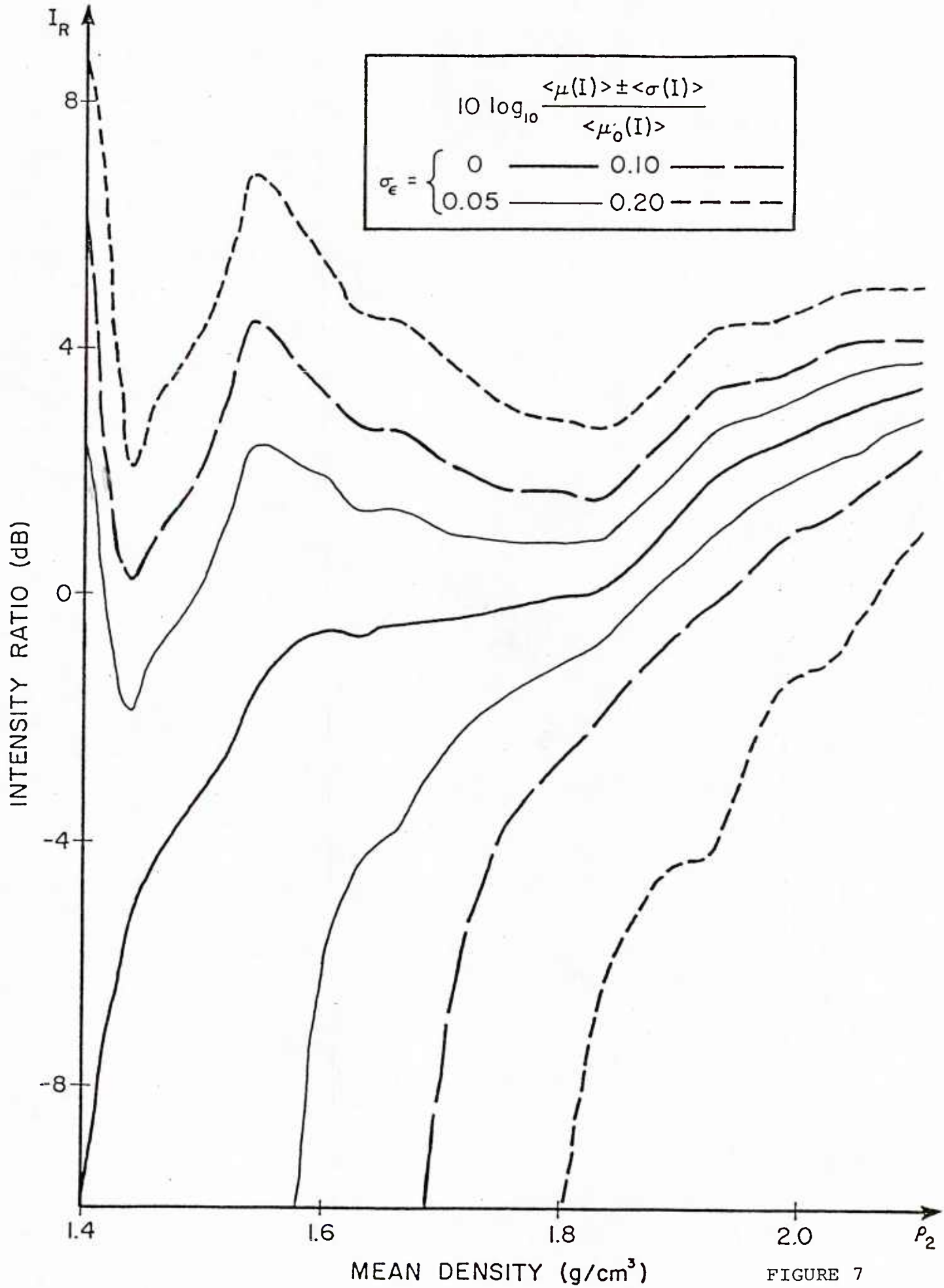
I_R
8
4
0
-4
-8
INTENSITY RATIO (dB)
$10 \log_{10} \frac{\langle \mu(I) \rangle \pm \langle \sigma(I) \rangle}{\langle \mu_0(I) \rangle}$
$\sigma_\epsilon = \begin{cases} 0 & \text{——} \; 0.10 \; \text{——} \; \text{——} \\ 0.05 & \text{——} \; 0.20 \; \text{– – – –} \end{cases}$
1.4
1.6
1.8
2.0
ρ_2
MEAN DENSITY (g/cm^3)

FIGURE 7

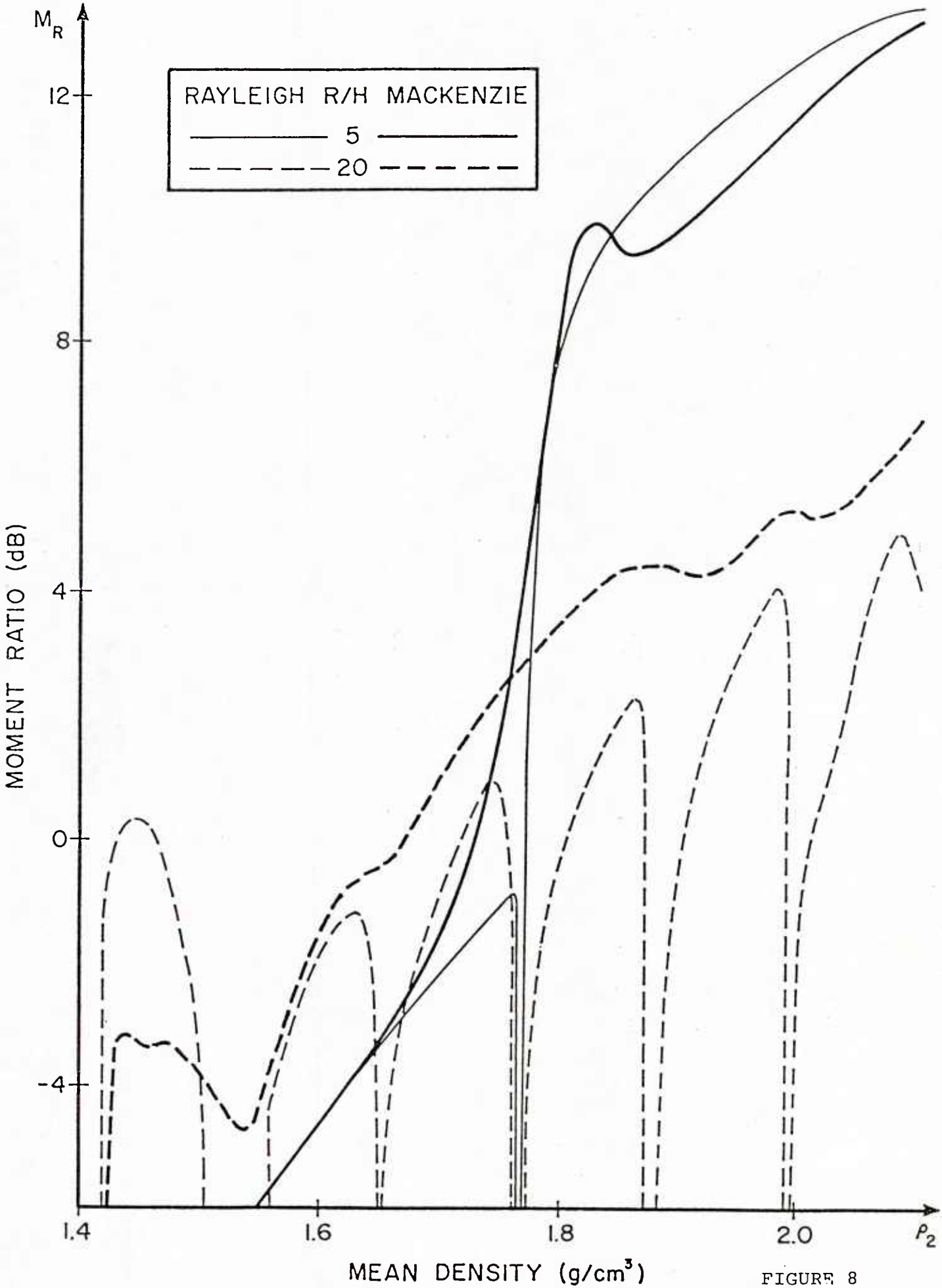
M_R
12
8
4
0
-4
RAYLEIGH R/H MACKENZIE
5
20
MOMENT RATIO (dB)
1.4
1.6
1.8
2.0
ρ2
MEAN DENSITY (g/cm³)

FIGURE 8

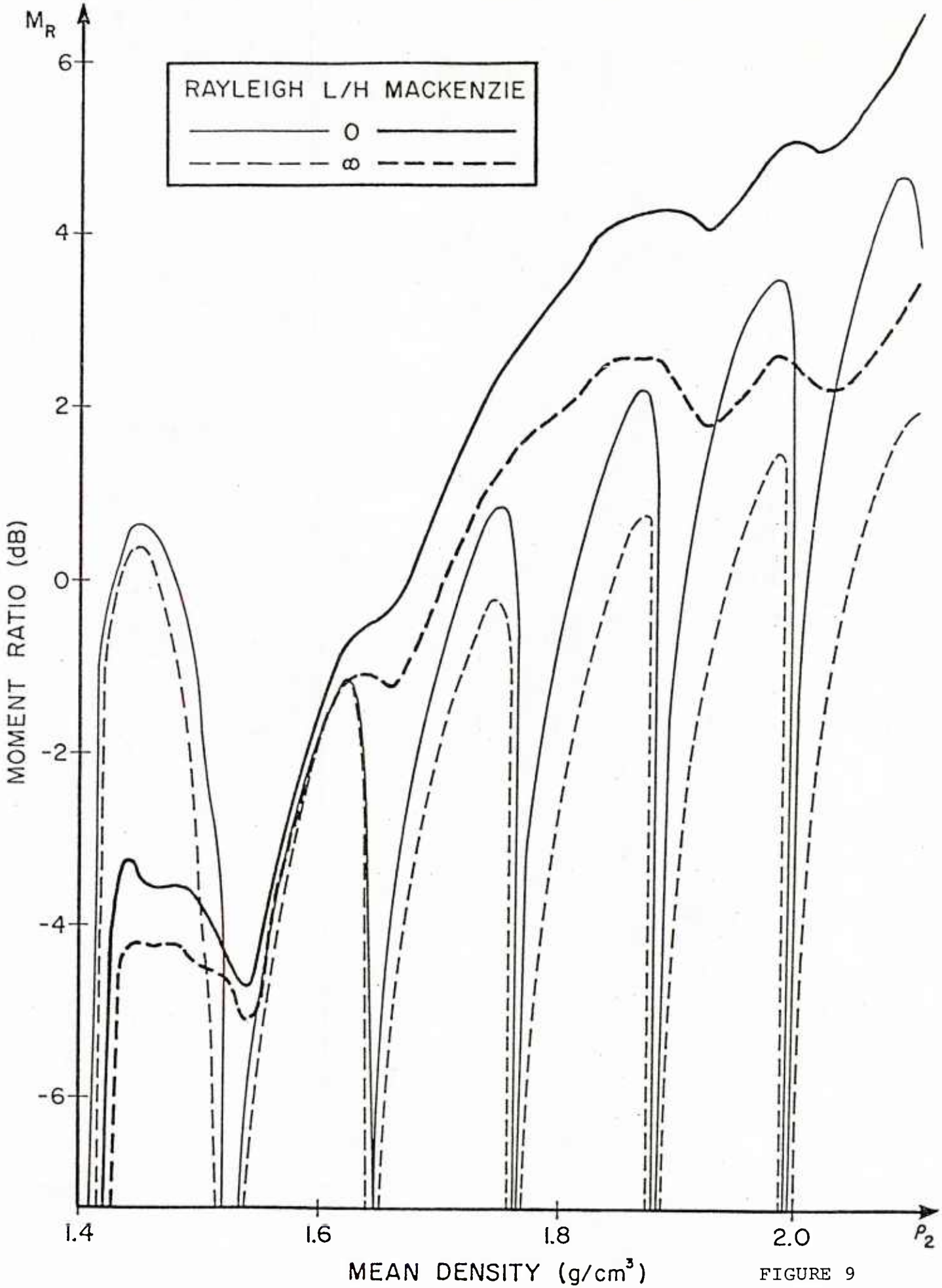
M_R
RAYLEIGH L/H MACKENZIE
0
∞
6
4
2
0
-2
-4
-6
MOMENT RATIO (dB)
1.4
1.6
1.8
2.0
P_2
MEAN DENSITY (g/cm³)

FIGURE 9

UNCLASSIFIED
DISTRIBUTION LIST
DEC 1981

Addressee	No. of Copies
Office of Naval Research 800 North Quincy Street Arlington, Virginia 22217	
Attn: Code 425AC	2
102	1
102C	1
210	1
220	1
Office of Naval Technology 800 North Quincy Street Arlington, Virginia 22217	
Attn: MAT 0721	1
MAT 0724	1
Director Naval Research Laboratory 4555 Overlook Avenue, SW. Washington, D.C. 20375	
Attn: Dr. J. C. Munson	1
Mr. R. R. Rojas	1
Dr. B. B. Adams	1
Dr. W. B. Moseley	1
Dr. J. P. Dugan	1
Unclassified Library	1
Superintendent Naval Research Laboratory Underwater Sound Reference Division P.O. Box 8337 Orlando, Florida 32806	1
Director Office of Naval Research Branch Office 1030 East Green Street Pasadena, California 91106	1
Office of Naval Research Rm 239, Campbell Hall University of California Berkeley, California 94720	1
Director Office of Naval Research Branch Office 495 Summer Street Boston, Massachusetts 02210	1
Office of Naval Research New York Area Office 715 Broadway - 5th Floor New York, New York 10003	1
Commanding Officer Office of Naval Research Branch Office Box 39 FPO New York 09510	1
Director Office of Naval Research Branch Office 536 South Clark Street Chicago, Illinois 60605	1
Office of Naval Research Resident Representative University District Building, Room 422 1107 North East 45th Street Seattle, Washington 98105	1

Addressee	No. of Copi
Technical Director Naval Oceanographic Research and Development Activity NSTL Station Bay St. Louis, Mississippi 39522	
Attn: Technical Director	1
Dr. L. Solomon	1
Dr. R. Gardner	1
Mr. E. Chaika	1
Mr. R. Van Wyckhouse	1
Dr. S. W. Marshall	1
Director Naval Oceanographic Office NSTL Station Bay St. Louis, Mississippi 39522	
Attn: Mr. H. Beck	1
Dr. T. M. Davis	1
Mr. W. H. Geddes	1
Dr. W. Jobst	1
Mr. R. Merrifield	1
Mr. R. A. Peloquin	1
Dr. M. K. Shank	1
Office of the Assistant Secretary of the Navy for Research, Engineering and Systems Washington, D.C. 20350	
Attn: Dr. D. Barbe, Rm 4E732 Pentagon	1
Dr. J. H. Probus, Rm 5E779 Pentagon	1
Chief of Naval Operations Room 5D580, Pentagon Washington, D.C. 20350	
Attn: OP951F	1
Commander Naval Sea Systems Command Department of Navy Washington, D.C. 20362	
Attn: Capt. James M. Van Metre PMS 409	1
Chief of Naval Operations Office of the Director Naval Oceanographic Division OP-952 Department of the Navy Washington, D.C. 20352	
Attn: Dr. R. W. James	1
Capt. J. C. Harlett	1
Commander Oceanographic System, Atlantic Box 100 Norfolk, Virginia 23511	1
Commander Oceanographic System, Pacific Box 1390 Pearl Harbor, Hawaii 96860	1

Addressee	No. of Copies
Defense Advanced Research Projects Agency 1400 Wilson Boulevard Arlington, Virginia 22209 Attn: Capt. V. Simmons	1
ARPA Research Center Moffett Field Unit #1 California 94035 Attn: Mr. E. Smith	1
Commanding Officer Fleet Weather Central Box 113 Pearl Harbor, Hawaii 96860	1
Naval Ocean Systems Center (Kaneohe) Kaneohe, Hawaii 96863 Attn: Mr. D. Hightower Mr. B. Kishimoto Mr. R. Buecher	1 1 1
Commander Naval Electronic Systems Command 2511 Jefferson Davis Highway National Center #1 Arlington, Virginia 20360 Attn: CAPT C. A. Rose,, PME 124 LCDR P. Girard, NAVELEX 612	2
Commander Naval Air Systems Command Jefferson Plaza #1 1411 Jefferson Davis Highway Arlington, Virginia 20360	1
Commander Naval Sea Systems Command National Center #2 2521 Jefferson Davis Highway Arlington, Virginia 20362 Attn: SEA 63R 63Y	1 1
Commanding Officer Fleet Numerical Weather Central Monterey, California 93940 Attn: Mr. Paul Stevens Dr. D.R. McLain (NMFS)	1 1
Defense Documentation Center Cameron Station Alexandria, Virginia 22314	12
Commander Naval Ocean Systems Center Department of the Navy San Diego, California 92132 Attn: Dr. Daniel Andrews Dr. Dean Hanna Mr. Henry Aurand Dr. Harry A. Schenck	1 1 1 1

Addressee	No. of Copi
Commander Naval Surface Weapons Center Acoustics Division Silver Spring, Maryland 20910	1
Commander Naval Surface Weapons Center Science and Mathematics Research Group (K05) Dahlgren, Virginia 22448 Attn: Dr. E.W. Schwiderski	1
Commanding Officer Naval Underwater Systems Center New London Laboratory New London, Connecticut 06320 Attn: Dr. William Von Winkle Dr. A. Nuttall Mr. A. Ellinthorpe Dr. D.M. Viccione Mr. A. Donn Cobb	1 1 1 1 1
Commander Naval Air Development Center Department of the Navy Warminster, Pennsylvania 18974 Attn: Unclassified Library	1
Commanding Officer Naval Coastal Systems Laboratory Panama City, Florida 32401 Attn: Unclassified Library	1
Commanding Officer Naval Underwater Systems Center Newport Laboratory Newport, Rhode Island 02840 Attn: Unclassified Library	1
Commander David W. Taylor Naval Ship Research and Development Center Bethesda, Maryland 20084 Attn: Dr. M. Sevik	1
Superintendent Naval Postgraduate School Monterey, California 93940	1
Superintendent U.S. Naval Academy Annapolis, Maryland 21402 Attn: Library	1
Commanding Officer Naval Intelligence Support Center 4301 Suitland Road Washington, D.C. 20390 Attn: NISC 20	1
Director Applied Physics Laboratory University of Washington 1013 North East 40th Street Seattle, Washington 98105 Attn: Dr. T.E. Ewart Dr. M. Schulkin	1 1

Addressee	No. of Copies
Applied Research Laboratories University of Texas at Austin P.O. Box 8029 10000 FM Road 1325 Austin, Texas 78712	
Attn: Dr. Loyd Hampton	1
Dr. Charles Wood	1
Atlantic Oceanographic and Meteorological Laboratories 15 Rickenbacker Causeway Miami, Florida 33149	
Attn: Dr. John Proni	1
Bell Telephone Laboratories 1 Whippany Road Whippany, New Jersey 07981	
Attn: Dr. Bruce Bogart	1
Dr. Peter Hirsch	1
Bolt, Beranek, and Newman, Inc. 50 Moulton Street Cambridge, Massachusetts 02238	
Attn: Dr. K. L. Chandiramani	1
Chase, Inc. 14 Pinckney Street Boston, Massachusetts 02114	
Attn: Dr. David Chase	1
Dr. David Middleton 127 East 91st Street New York, New York 10028	1
Duke University Department of Electrical Engineering Durham, North Carolina 27706	
Attn: Dr. Loren Nolte	1
General Electric Company Heavy Military Electronic Systems Syracuse, New York 13201	
Attn: Mr. Don Winfield	1
General Electric Company P.O. Box 1088 Schenectady, New York 12301	
Attn: Dr. Thomas G. Kincaid	1
Gould, Incorporated Chesapeake Instrument Division 6711 Baymeadow Drive Glen Burnie, Maryland 21061	
Attn: Dr. O. Lindemann	1
G R Associates, Inc. 10750 Columbia Pike Suite 602 Silver Spring, Maryland 20901	
Attn: Dr. Sheldon Gardner	
Dr. Frank Rees	
Hughes Aircraft Company P.O. Box 3310 Fullerton, California 92634	
Attn: Mr. S. W. Autrey	1

Addressee	No. of Copies
Hydroacoustics, Inc. 321 Northland Ave. P.O. Box 3818 Rochester, New York 14610	1
Institute for Acoustical Research Miami Division for the Palisades Geophysical Institute 615 South West 2nd Avenue Miami, Florida 33130	
Attn: Mr. M. Kronengold	1
Dr. J. Clark	1
Institute of Geophysics and Planetary Physics Scripps Institute of Oceanography University of California La Jolla, California 92093	
Attn: Dr. W. Munk	1
Mr. J. Spiesberger	1
Jaycor Incorporated 205 South Whiting Street Suite 607 Alexandria, Virginia 22304	
Attn: Dr. S. Adams	1
Massachusetts Institute of Technology Acoustics and Vibration Laboratory 70 Massachusetts Avenue Room 5-222 Cambridge, Massachusetts 02139	
Attn: Professor Patrick Leehey	1
Palisades Sofar Station Bermuda Division of Palisades Geophysical Institute FPO New York 09560	
Attn: Mr. Carl Hartdegen	1
Polar Research Laboratory 123 Santa Barbara Avenue Santa Barbara, California 93101	
Attn: Mr. Beaumont Buck	1
Research Triangle Institute Research Triangle Park Durham, North Carolina 27709	
Attn: Dr. S. Huffman	1
Rensselaer Polytechnic Institute Troy, New York 12181	
Attn: Dr. Melvin J. Jacobson	
Science Applications, Inc. 8400 Westpark Drive McLean, Virginia 22102	
Attn: Dr. P. Tatro	
S.D.P. Inc. 15250 Ventura Boulevard Suite 518 Sherman Oaks, California 91403	
Attn: Dr. M. A. Basin	1

Addressee	No. of Copies
Texas Instruments, Inc. 13500 North Central Expressway Dallas, Texas 75231 Attn: Mr. Charles Black	1
Underwater Systems, Inc. 8121 Georgia Avenue Silver Spring, Maryland 20910 Attn: Dr. M. Weinstein	1
University of Miami Rosenstiel School of Marine and Atmospheric Sciences 4600 Rickenbacker Causeway Miami, Florida 33149 Attn: Dr. H. DeFerrari	1
University of Michigan Department of Aerospace Engineering, North Campus Ann Arbor, Michigan 48109 Attn: Dr. W. W. Wilmarth	
University of Michigan Cooley Electronics Laboratory Ann Arbor, Michigan 48105 Attn: Dr. T. G. Birdsall	
University of Rhode Island Department of Electrical Engineering Wakefield, Rhode Island 02881 Attn: Dr. Donald Tufts	1
Woods Hole Oceanographic Institution Woods Hole, Massachusetts 02543 Attn: Dr. Paul McElroy Dr. R. Spindel	1 1